Research Square

Preprints are preliminary reports that have not undergone peer review.
They should not be considered conclusive, used to inform clinical practice,
or referenced by the media as validated information.

Piperazine-Based Dinuclear Transition Metal Complexes as Potential Metallopharmaceutical Scaffolds: Synthesis, Protein Binding, Cytotoxicity and Molecular Modeling

Ritika Saini
Lovely Professional University
Rishi Kant
GNA University
Sourbh Suren Garg
Lovely Professional University Phagwara
Suman Maji
suman.18432@lpu.co.in

Lovely Professional University

Research Article

Keywords: piperazine-based ligands, dinuclear complexes, BSA binding, cytotoxicity, antibacterial activity

Posted Date: November 24th, 2026

DOI: https://doi.org/10.21203/rs.3.rs-11734752/v1

License: This work is licensed under a Creative Commons Attribution 4.0 International License.
Read Full License

Additional Declarations: No competing interests reported.

Piperazine-Based Dinuclear Transition Metal Complexes as Potential Metallopharmaceutical Scaffolds: Synthesis, Protein Binding, Cytotoxicity and Molecular Modeling

Ritika Saini[1], Rishi Kant[2] Sourbh Suren Garg[3], and Suman Maji[1]*

[1]*School of Chemical Engineering and Physical Sciences, Lovely Professional University Phagwara, Punjab-144411, India*

[2]*School of Natural Science, GNA University, Phagwara (Punjab), 144401, India*

[3]*Department of Biochemistry, School of Bioengineering and Biosciences, Lovely Professional University Phagwara, Punjab-144411, India*

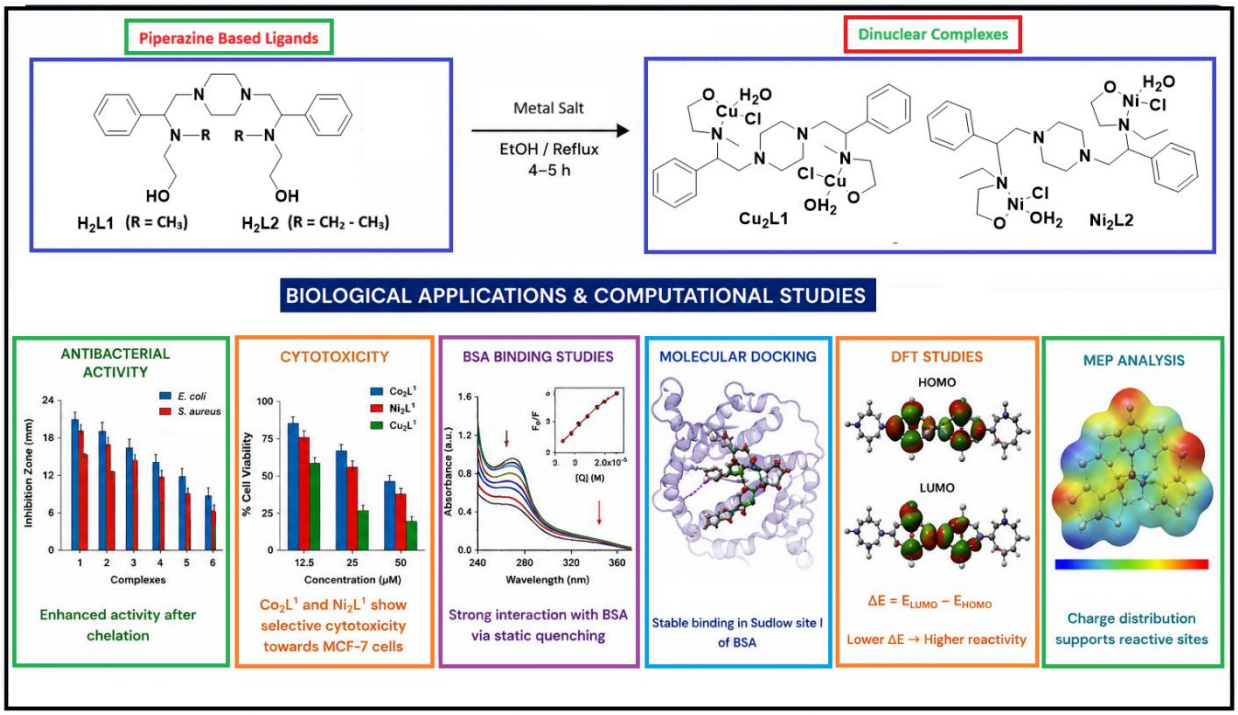
*Corresponding author, e-mail: suman.18432@lpu.co.in

Abstract:

Dinuclear complexes functionaslised with piperazine-based multidentate ligands have gained considerable attention owing to their cooperative metal-centered reactivity and promising biomedical potential. In the present study, two novel piperazine-derived ligands containing dual coordination sites were synthesized through epoxide ring opening, chlorination, and subsequent substitution with selected secondary amines. These ligands were further complexed with Cu(II), Co(II), and Ni(II) ions to afford a series of binuclear metal complexes. The synthesized ligands and complexes were comprehensively characterized using FT-IR, UV-Visible, EPR, ^{1}H-NMR, ^{13}C-NMR spectroscopy, mass spectrometry, and thermogravimetric analysis. Spectroscopic investigations confirmed successful coordination of metal ions through nitrogen and oxygen donor atoms. EPR (isotropic, g = 2.16-2.2) and electronic spectral studies suggested significant ferromagnetic metal–metal interactions and distorted coordination geometries in Cu(II) complexes. Thermal analyses indicated the presence of coordinated water molecules (losses at 80-150°C) and enhanced thermal stability of the complexes. Geometry optimization and electronic structure investigations were further supported by computational studies. The biomedical significance of the newly synthesized compounds was studied via antibacterial, cytotoxicity, Bovine Serum Albumin (BSA) binding and molecular docking studies. There was significant enhancement in antibacterial properties by the complexes in comparison to free ligands. Among the compounds, Cu(II) complexes showed the highest inhibitory activity against both Gram-positive, *E. coli* (up to

25.8 mm) and Gram-negative, *S. aureus* (up to 22.6 mm). This may be attributed to increased lipophilicity and improved membrane permeability upon chelation. In vitro cytotoxicity studies revealed selective anticancer activity toward MCF-7 breast cancer cells (IC_{50} 12-51 µg/mL) with comparatively lower toxicity toward normal BHK-21 cells (IC_{50} >150 µg/mL). UV–Visible absorption titration studies indicated moderate binding affinity of the complexes toward BSA, supporting their potential biomolecular transport behavior, while molecular docking studies further validated favorable protein–ligand interactions at the binding site. The integrated spectroscopic, computational, and biological results suggest that these piperazine-based dinuclear metal complexes represent promising scaffolds for the development of biologically active metallopharmaceutical agents.

Keywords: piperazine-based ligands, dinuclear complexes, BSA binding, cytotoxicity, antibacterial activity.



Graphical Abstract Text: Two new piperazine-based ligands and their Cu(II), Co(II), Ni(II) complexes were synthesized and characterized. Studies show complexation enhanced antibacterial activity (Cu_2L2 vs *E. coli* 25.8 mm; Cu_2L1 vs *S. aureus* 21.9 mm) Cytotoxicity assays revealed strong anti-proliferative effects on MCF-7 cells with lower IC_{50} values (12–51) and reduced toxicity on normal BHK-21 cells (150–250), highlighting anticancer potential.

BSA binding (10–128 M^{-1}) and docking confirmed favorable protein interactions, supporting drug delivery prospects.

Highlights:

- Novel piperazine-based binuclear metal complexes were synthesized.
- FMO and MEP analyses revealed enhanced electronic reactivity.
- Metal coordination significantly improved antibacterial activity.
- Complexes exhibited selective cytotoxicity against MCF-7 cells.
- Molecular docking supported stable BSA–complex interactions.

1. Introduction

Multinuclear transition metal complexes have attracted increasing attention in coordination and medicinal chemistry because of their cooperative metal-centered reactivity, structural diversity, and enhanced biomolecular interactions. Among these systems, dinuclear complexes supported by multidentate ligands exhibit promising physicochemical and biological properties [Li et al., 2020]. The term "dinucleating ligands" was introduced in 1970 by Robson to describe polydentate chelating systems capable of simultaneously coordinating two metal centers. Since then, a wide variety of multidentate ligands and their metal complexes have been synthesized and extensively studied for their biological and pharmacological application [Nekrasov, 2001]. Nitrogen-containing heterocycles have earned significant scientific attention in recent decades due to their prominent therapeutic properties [Shebl, 2014]. In particular, piperazine-based ligands have attracted significant attention in coordination chemistry because of the diverse coordination behavior and therapeutic potential of their metal complexes [Chandra et al., 2009; Kant and Maji, 2021; Bhati et al., 2019]. Piperazine derivative and their metal complexes have been reported to diverse pharmacological activities as antibiotics, anticancer, antitumor, antimicrobial, antipsychotics and antidepressants properties [Kumar et al., 2014; Asif, 2015; Sharma and Makkar, 2017; Chaudhary et al., 2006]. Piperazine contains two nitrogen donor atoms positioned opposite to each other within the heterocyclic ring and behaves as a weak base. Substitution on both nitrogen atoms can result

in piperazine-based ligands having unique structural feature and versatile metal binding properties suitable for various applications.

Several studies have demonstrated that piperazine-based multidentate ligands and Schiff base ligands readily form stable complexes with transition metal ions such as Cu(II), Co(II), and Ni(II). These metal complexes have shown biomolecular interaction capabilities, including DNA/protein binding affinity, redox-mediated cytotoxicity, and enhanced DNA-binding potential [Kant et al., 2020; Mondal et al., 2023]. M. Pait et al. reported Cu(II) complexes of piperazine based ligand which shows significant anticancer activity and BSA-binding affinity [Pait et al., 2014]. K. Babu et al. synthesized Cu(II), Co(II), Zn(II) and Ni(II) complexes derived from the tetradentate ligand and evaluated their biological activities [Babu and Pitchai, 2014]. R. Kant et al. reported piperazine based mononuclear and binuclear complexes exhibiting notable antifungal, antibacterial, and cytotoxic activities [Kant and Maji, 2021; Kant et al., 2020; Kant and Maji, 2023]. M.S. Ragab et al. synthesized biologically active Co(II), Cu(II), and Zn(II) Schiff base complexes exhibiting notable cytotoxicity, DNA cleavage activity, and favorable protein-binding interactions [Ragab et al., 2022]. M. S. Ahmad et al. synthesized binuclear Cu(II) complexes exhibiting significant antimicrobial and cytotoxic activities against the MCF-7 cell line, supported by crystallographic and spectroscopic characterization [Ahmad et al., 2021]. H. Keypour et al. synthesized a piperazine-containing hexaaza Schiff base Ni(II) complex with distorted octahedral where combined biological and DFT/NBO investigations demonstrated notable anticancer and antioxidant activities [Keypour et al., 2023]. M. Das et al. reported piperazine-derived Cu complexes exhibiting strong DNA/protein binding affinity and significant anticancer activity, particularly for the Cu(II) complex, which was associated with enhanced reactive oxygen species generation [Das et al., 2025]. Recently our group reported the binuclear copper complexes of piperazine based ligands exhibiting promising antimicrobial, BSA binding and anticancer activities highlighting the potential of such systems for further medicinal coordination chemistry [Kant and Maji, 2024].

Despite significant progress in piperazine-based coordination chemistry, studies involving structurally flexible dinuclear systems possessing dual coordination environments remain relatively limited. Furthermore, comprehensive investigations integrating spectroscopic characterization, computational analysis, biomolecular interaction studies, and biological evaluation for establishing structure–activity relationships are still underexplored [Gokturk et

al., 2023; Kant et al., 2024; Malav and Ray, 2025; Keypour et al., 2017; Keypour et al., 2008]. In the present work, two new piperazine-based multidentate ligands were synthesized through a three-step reaction sequence involving epoxide ring opening, followed by chlorination and subsequent condensation with secondary amines. These ligands were further employed for the synthesis of binuclear Cu(II), Co(II), and Ni(II) complexes. The present study aims to establish possible structure–activity relationships through comprehensive spectroscopic, computational, and biological investigations of these complexes and to evaluate their potential as bioactive metallopharmaceutical candidates with antimicrobial and anticancer relevance.

2. Experimental Section

2.1 Materials and Methods:

All chemicals and solvents required for the study were purchased from Sigma -Aldrich, Loba Chemie Pvt. Ltd. (AR Grade) and were used as received. Solvents were stored over molecular sieve 3A. UV-visible absorption spectra were recorded on Shimadzu UV-1800 in the wavelength range 200-800 nm. Shimadzu FTIR 8400 spectrometer with diamond ATR was used to record IR in the range 400-4000 cm^{-1}. For recording 1H-NMR spectra JEOL JNM-ECS-400 was used with d^6-DMSO/$CDCl_3$ as solvents with tetra methyl silane (TMS) as the internal standard. Mass Q-ToF Micro Waters (LCMS) was used to determine the molecular mass of compound. MiniScope MS-5000 bench top EPR/ESR Spectrometer was used for the for collecting EPR signal in the X band.

2.2 Synthesis of intermediate ligand 2,2'-(piperazine-1,4-diyl)bis(1-phenylethane-1-ol) (E1)

The intermediate 2,2'-(piperazine-1,4-diyl)bis(1-phenylethane-1-ol) (E1) was prepared by the stirring of 15 mmol (1.29g) of piperazine with 30 mmol (3.6g) of styrene oxide in ethanol at low temperature (0°C) [22]. This reaction mixture was refluxed for 14 hours, and reaction progress was analyzed by TLC ($CHCl_3$: MeOH). A white precipitate was obtained and dried in vacuum desiccator (scheme 1). Recrystallization was done by using hot chloroform. Physical state solid, white colour, yield 68%, m. pt. 268°C, FT-IR (υ in cm^{-1}) 3143 (O-H str.) 2920 (C-H str.), 1393 (C-N str.), 2828 (aromatic C-H str.), C=C 1452 (aromatic C=C str.), ^{1}H-NMR ($CDCl_3$, δ, ppm) 1.60 (4H, triplet, CH_2), 2.53 (2H, doublet, CH_2), 2.84 (1H, multiplet,

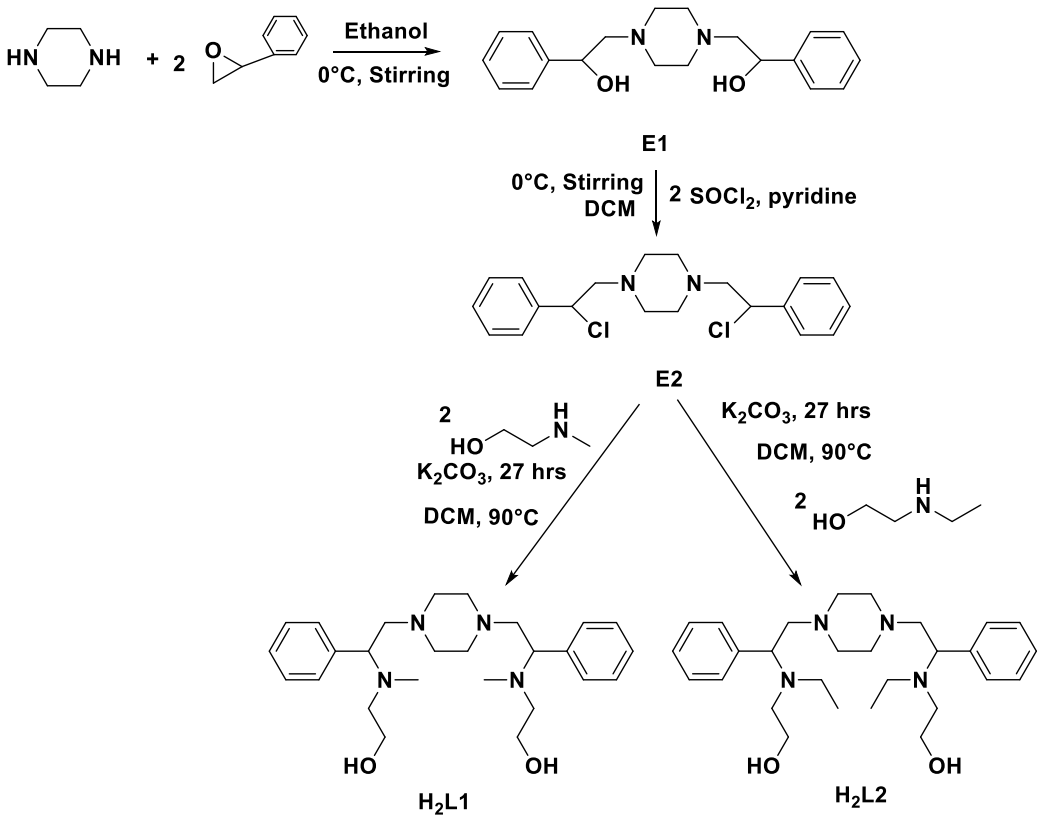
CH), 4.73 (1H, singlet, OH), 7.36 (2H, doublet, Ar-H), 7.34 (2H, singlet, Ar-H), 7.29 (H, doublet, Ar-H), ^{13}C-NMR ($CDCl_3$, δ, ppm) 66.19 (CH_2), 68.85 (CH_2), 68.82 (CH), 142.02 (aromatic CH), 125.95 (aromatic CH), 128.50 (aromatic CH), 127.69 (aromatic CH), Mass spectra (m/z) 327 ,UV-Vis (λ_{max}) 457 nm.

2.3 Synthesis of intermediate ligand 1,4-bis(2-chloro-2-phenylethyl)piperazine (E2)

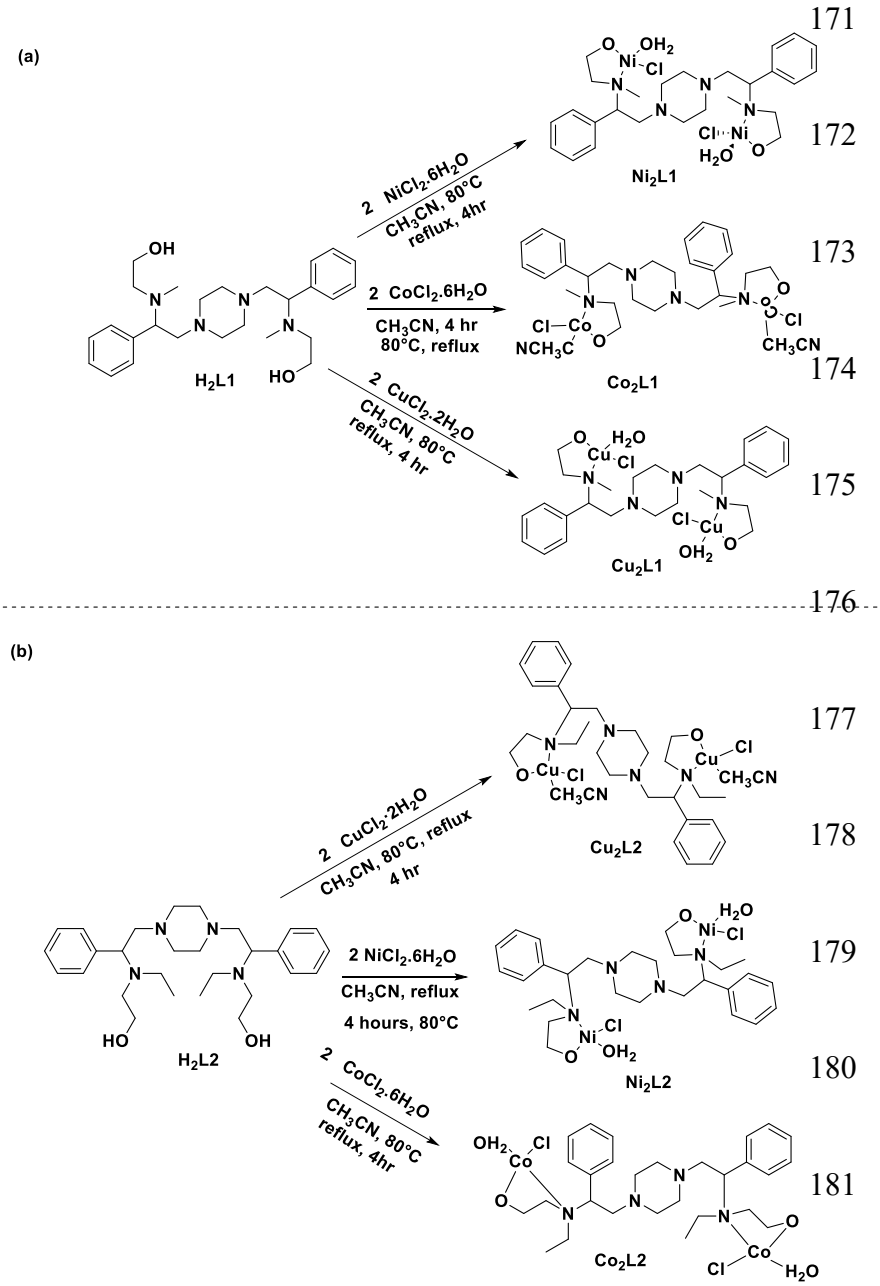
Intermediate (E2) was prepared by the addition of 2.32 ml of $SOCl_2$ and 2 ml of pyridine in 1g of 2,2'-(piperazine-1,4-diyl)bis(1-phenylethane-1-ol) (E1) in DCM at low temperature(0°C) [23]. This reaction mixture was refluxed for 13 hours and reaction progress was confirmed by TLC (hexane: ethyl acetate). An amber yellow colour precipitate was obtained and precipitate was filtered by vacuum pump (scheme 1). Physical state solid, amber yellow colour, yield 74%, m. pt. 235°C, FT-IR (υ in cm^{-1}) 2990 (C-H str.), 1263 (C-N str.), 1428 (aromatic C=C str.), 773 (C-Cl vib.), ^{1}H-NMR (DMSO-d6, δ, ppm) 3.49 (4H, triplet, CH_2), 3.14 (2H, doublet, CH_2) 4.82 (1H, multiplet, CH), 7.59 (2H, doublet, Ar-H), 7.36 (1H, singlet, Ar-H) 7.40 (2H, doublet, Ar-H), ^{13}C-NMR (DMSO-d6, δ ppm) 56.49 CH2, 129.32 CH, 126.60 aromatic CH, 127.43 aromatic CH, 129.32 aromatic CH, Mass spectra (m/z) 363, 365, 345, 327, 309, 189, UV-Vis (λ_{max}) 256 nm.

2.4 Synthesis of 2,2'-((piperazine-1,4-diylbis(1-phenylethane-2,1-diyl))bis(methylazanediyl))bis(ethan-1-ol) (H_2L1)

Ligand (H_2L1) was prepared by the condensation of 2.7mmol of E2 with 5.4 mmol of 2-(methylamino)ethanol and 10 mmol of potassium carbonate in DCM at 90°C temperature (scheme 1). This reaction mixture was refluxed for 27 hours and analysed by TLC ($CHCl_3$:MeOH). A yellow oily compound was obtained. Physical state: liquid, yellowish colour, yield 53%, FT-IR (υ in cm^{-1}) 3400 (O-H str.), 2935 (C-H str.), 1370, 1397 (C-N str.), 1624 (aromatic C=C str.), 1122 (C-O str.), ^{1}H-NMR ($CDCl_3$, δ, ppm) 2.90 (4H, triplet, CH_2), 3.03 (2H, doublet CH_2), 2.31 (1H, multiplet, CH), 7.14 (2H, doublet, Ar-H), 7.32 (2H, singlet, Ar-H),8.09 (1H, doublet, Ar-H), 1.24 (6H, singlet, CH_3) , 3.36 (2H, doublet, CH_2), 3.79 (2H, doublet, CH_2) ,4.66 (1H, singlet, OH) ^{13}C-NMR ($CDCl_3$, δ, ppm) 60.82 (CH_2), 60.37 (CH_2), 59.32 (CH_2), 69.90 (CH),125.93 (Ar CH), 142.02 (Ar CH), 128.95 (Ar CH), 127.63 (Ar CH), 36.04 (CH_3), 51.91 (CH_2), 48.01 (CH_2), Mass spectra (m/z) 441, 411, 384, 290, 206, 112, UV-Vis (λ_{max}) 211 nm.



Scheme 1. Synthesis of intermediate ligands (E1-E2) and multidentate ligands H_2L1 and H_2L



Scheme 2. Synthetic scheme for (a) Binuclear complexes of H_2L1 and (b) Binuclear complexes of H_2L2

2.5 Synthesis of 2,2'-((piperazine-1,4-diylbis(1-phenylethane-2,1-diyl))bis(ethylazanediyl))bis(ethan-1-ol) (H_2L2)

Ligand (H_2L2) was prepared by the general method as mentioned for H_2L1 with 11.2 mmol of 2-(ethylamino)ethanol. A brown oily compound was obtained after 27 hours (scheme 1). Physical state: brown oily compound, yield 59%, FT-IR (υ in cm^{-1}) 3127 (O-H str.), 2914 ,2823

(C-H str.), 1449, 1322 (C-N str.), 1164 (C-O str.), 1664 (Ar. C=C str.), ^{1}H-NMR ($CDCl_3$, δ, ppm) 2.70 (4H, triplet, CH_2), 2.41 (2H, doublet, CH_2), 4.03 (1H, multiplet, CH), 7.26 (2H, doublet, Ar-H), 7.30 (2H, singlet, Ar-H), 7.10 (1H, doublet, Ar-H), 1.18 (2H, doublet, CH_2), 3.81 (2H, doublet, CH_2), 5.02 (1H, singlet, OH), 2.28 (2H, doublet, CH_2), 1.05 (6H, triplet, CH_3), ^{13}CNMR ($CDCl_3$, δ, ppm) 60.53 (CH_2), 66.12 (CH_2), 68.71 (CH), 142 (CH), 128.86 (Ar CH), 127.52 (Ar CH), 125.83 (Ar CH), 47.38 (CH_2), 65.22 (CH_2), 12.40 (CH_3), 44.91(CH_2), Mass spectra (m/z) 468, UV-vis (λ_{max}) 207 nm.

2.6 General method for binuclear complexes of H_2L1 and H_2L2

The binuclear complexes of ligands H_2L1 and H_2L2 were obtained by the mixing of 1 mmol of ligand with 2 mmol of metal salt in 20 ml of acetonitrile (scheme 2). The reaction mixture was refluxed on a magnetic stirrer for about 4 hours and at the end of reaction, precipitates are obtained and separate out under vacuum. These synthesized compounds were recrystallized by methanol solvent. The precipitates were dried in vacuum desiccator.

$[Cu_2(L1)Cl_2(H_2O)]$ Cu_2L1: Physical state: green solid compound, yield 72%, m. pt. 298°C, FT-IR (υ in cm^{-1}) 2974, 2823(C-H str.), 1631 (C=C str.), 1374, 1322 (C-N str.), 1077,1004 (C-O str.), 821 (Cu-Cl str.), 697(Cu-N str.), 662 (Cu-O), Mass spectra (m/z) 710, 634, 560, 336, 262, UV-Vis (λ_{max}) 215, 267 nm, EPR (g value) 2.16.

$[Co_2(L1)Cl_2(CH_3CN)_2]$ Co_2L1: Physical state: violet solid compound, m. pt. 289°C, yield 92%, FT-IR (υ in cm^{-1}) 2993 (C-H str.), 1458, 1322 (C-N str.), 1058 (C=C str.), 835 (Co-Cl str.), 717 (Co-N str.), 519 (Co-O str.), Mass spectra (m/z) 710, 634, 560, 466, 336, UV-Vis (λ_{max}) 218, 270 nm.

$[Ni_2(L1)Cl_2(H_2O)_2]$ Ni_2L1: Physical state: green solid compound, m. pt. 282°C, yield 54%, FT-IR (υ in cm^{-1}) 3359 (lattice O-H str.), 2974 (C-H str.), 1626 (C=C str.), 1389,1322 (C-N str.), 1063 (C-O str.), 830 (Ni-Cl str.), 697 (Ni-N str.), 470 (Ni-O str.), Mass spectra (m/z) 685, 551, 473, 355, 201, UV-Vis (λ_{max}) 220, 268 nm.

$[Cu_2(L2)Cl_2(CH_3CN)_2]$ Cu_2L2: Physical state: green solid compound, yield 79%, m. pt. 293°C, FT-IR (υ in cm^{-1}) 2964, 2990 (C-H str.), 1631 (C=C str.), 1361(C-N str.), 1050 (C-O

str.), 820 (Cu-Cl str.) 702 (Cu-N str.), 404 (Cu-O str.) Mass spectra (m/z) 745, 644, 543, 442, 341, 240, UV-Vis (λ_{max}) 219, 265 nm, EPR (g value) 2.2.

$[Co_2(L2)Cl_2(H_2O)_2]$ Co_2L2: Physical state: violet solid compound, m. pt. 296°C, yield 86%, FT-IR (υ in cm^{-1}) 3552 (lattice O-H str.), 2991 (C-H str.), 1636 (C=C str.), 1393 (C-N str.), 1058 (C-O str.), 831 (Co-Cl str.) , 702 (Co-N str.), 420 (Co-O str.), Mass spectra (m/z) 713, 486, 360, 327, 189, UV-Vis (λ_{max}) 219, 268 nm.

$[Ni_2(L2)Cl_2(H_2O)_2]$ Ni_2L_2: Physical state: green solid compound, m. pt. 275°C, yield 60%, FT-IR (υ in cm^{-1}) 2990(C-H str.), 1406 (C=C str.), 1259 (C-N str.), 1621 (O-H vib.), 1058 (C-O str.), 850 (Ni-Cl str.), 702 (Ni-N str.), 457(Ni-O str.), Mass spectra (m/z) 710, 421, 103, 189, 127, UV-Vis (λ_{max}) 213, 245 nm.

3. Results and Discussion

3.1 FT-IR spectral analysis

In the FT-IR spectra, broad absorption band observed in the region of 3100-3400 cm^{-1} were attributed to indicate the O-H stretching vibrations of the ligands E1, H_2L1 and H_2L2 [Bhat and Tabassum, 2009]. The C-N stretching band were observed in the region of 1390-1250 cm^{-1} for ligands and complexes [Otieno et al., 1995]. The band in the region of 3000-2800 cm^{-1} and 1400–1600 cm^{-1} were assigned to aliphatic C-H stretching and aromatic C=C stretching vibrations, respectively, in all ligand and complexes [Sodanapalli and Nair, 2011]. A band was observed in the region of 773 cm^{-1} which is characteristic to C-Cl bond of E2 [Ruede and Thornton, 1976]. In addition, C-O stretching band was observed in the region of 1170-1050 cm^{-1} in the spectra of ligands and complexes [Smith, 2017]. In the absence of single-crystal X-ray diffraction data, FT-IR analysis provides important insight into the coordination behavior and binding modesof the ligands to the metal complex [Alaghaz and Ammar, 2010; Alaghaz et al., 2013]. he appearance of new bands in the regions 898–820 cm^{-1}, 820–640 cm^{-1}, and 702–420 cm^{-1} were assigned to ν(M–Cl), ν(M–N), and ν(M–O) vibrations, respectively, confirming successful coordination of the ligands with the metal ions and formation of the corresponding complexes [Turkyilmaz, 2017]. road absorption bands in the region 3600–3300 cm^{-1} observed for all metal complexes indicated the presence of coordinated and/or lattice

water molecules [Dong et al., 2009]. The FT-IR spectra of ligands and complexes have been provided in supplementary file (Fig. S1 – S10) and selected bond frequencies are shown in table 1.

Table 1. Selected bond frequencies (cm^{-1}) of ligands and complexes

Compound	O-H	C-H	C-N	C=C	C-O	M-N	M-O	M-Cl
E1	3049	2991	1393	1457	1078	-	-	-
E2	-	2990	1263	1428	-	-	-	-
H_2L1	3400	2935	1397,1370	1624	1122	-	-	-
H_2L2	3127	2914,2823	1322	1664,1449	1164	-	-	-
Cu_2L1	-	2974	1374	1631	1077,	697	662	821
Co_2L1	3374	2978	1344	1566, 1467	1068	757	646	855
Ni_2L1	3359	2974	1389	1626	1063	697	470	830
Cu_2L2	-	2994	1361	1631	1050	702	494	820
Co_2L2	3552	2991	1393	1636	1058	702	420	831
Ni_2L2	3665	2990	1259	1406	1058	702	457	850

3.2 NMR spectral analysis

In the ^{1}H-NMR of the E1, H_2L1 and H_2L2 obtained in deuterated chloroform ($CDCl_3$) while that of E2 was obtained in deuterated dimethylformamide (d^6-DMSO). In the comparative observation, a signal at 1.58-2.90 ppm in ligands spectra were found due to (CH_2) protons of piperazine ring. The CH protons were observed in the range 3.00-4.60 ppm while OH protons were observed in the range 4.72-5.15 ppm. The multiplet in the range of 7.3- 7.51 ppm was assigned to protons of aromatic ring while a singlet was observed in the range of 1.05-1.25 ppm due to alkyl group. The ^{1}H-NMR spectrum of ligand H_2L1 is shown in figure 1, while the spectra of E1, E2, and H_2L2 are provided in the supplementary material. (figure S11–S13). In the ^{1}H-NMR spectrum of ligand H_2L1, the protons labeled ‘a’ appear as a triplet at 2.90 ppm, integrating for four protons. The two protons marked as ‘b’ exhibit a doublet at an upfield value of 2.48 ppm. Proton labeled ‘c’ shows a multiplet splitting at an upfield region around 3.79 ppm. The two protons marked as ‘d’ show a slight downfield shift, appearing as a doublet at 7.14 ppm, while the protons labeled ‘e’ appear as a singlet at 7.32 ppm. A single proton

marked as ‘f’ appears as a doublet at the upfield value of 8.09 ppm. Three protons assigned as ‘g’ show a singlet at 1.24 ppm. At 3.36 ppm, the signal labeled ‘h’ appears as a doublet corresponding to two protons. Protons assigned ‘i’ at 3.79 ppm, integrating two protons. A broad singlet at 4.66 ppm, labeled ‘j’, corresponds to one proton and is attributed to the –OH groups present in the ligand.

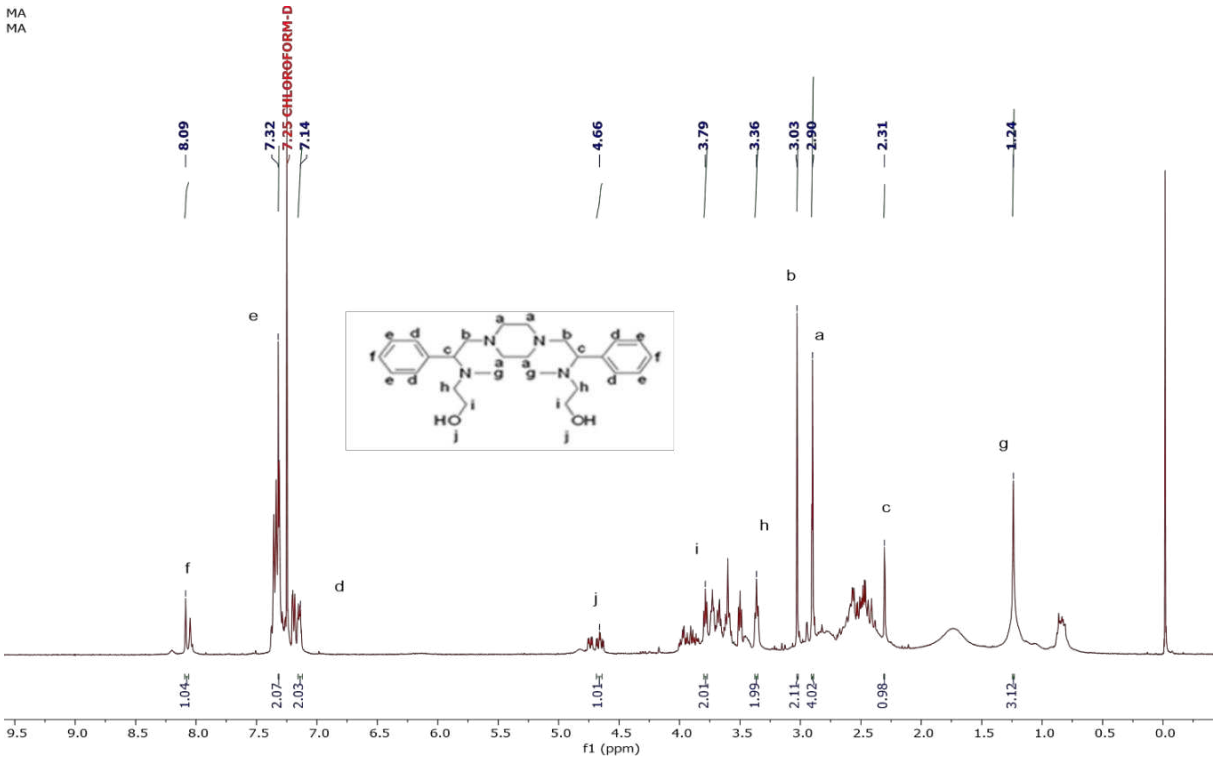


Figure 1. 1H-NMR spectra of multidentate ligand (H_2L1)

Similar to ^{1}H NMR, ^{13}C-NMR of the E1, H_2L1 and H_2L2 were analyzed in chloroform ($CDCl_3$) while that of E2 was analyzed in d6-DMSO. In the comparative observation a signal at 57-66 ppm in ligand spectra was due to piperazine ring and (CH_2) protons. The CH protons was observed in the range 66-68 ppm. The multiplet in the range of 125-142 ppm was assigned to carbons of benzene rings while a singlet at 12.40-22.90 ppm was due to methoxy group of the ligands. The 13C-NMR spectra of ligand H_2L1 is shown in the figure 2 while that of E1, E2, and H_2L2 are given in the supplementary file (figure S14 –S16). In ^{13}C-NMR spectra of ligand H_2L1, a peak is observed at 60.82 and 60.37 ppm which is marked as ‘a’. While the peak ‘b’ observed at 59.32 ppm and ‘c’ point shows at 69.90 ppm. Aromatic carbon is present and marked as ‘d’, ‘e’, ‘f’ and ‘g’ which shows peaks in the region of 120-142 ppm. Point ‘d’

shows at 142.01 ppm where peak e' shows at the region of 128.95. Point 'f' shows at 127.63 ppm and peak 125.93 ppm marked as 'g'. Point 'h' shows at 36.04 ppm, point 'i' shows at 51.91 ppm and 'j' point shows at the region of 48.01 ppm. Thus, ^{13}C-NMR spectra show also good agreement of proposed structure of ligand representing the carbon peaks matching with the fragment.

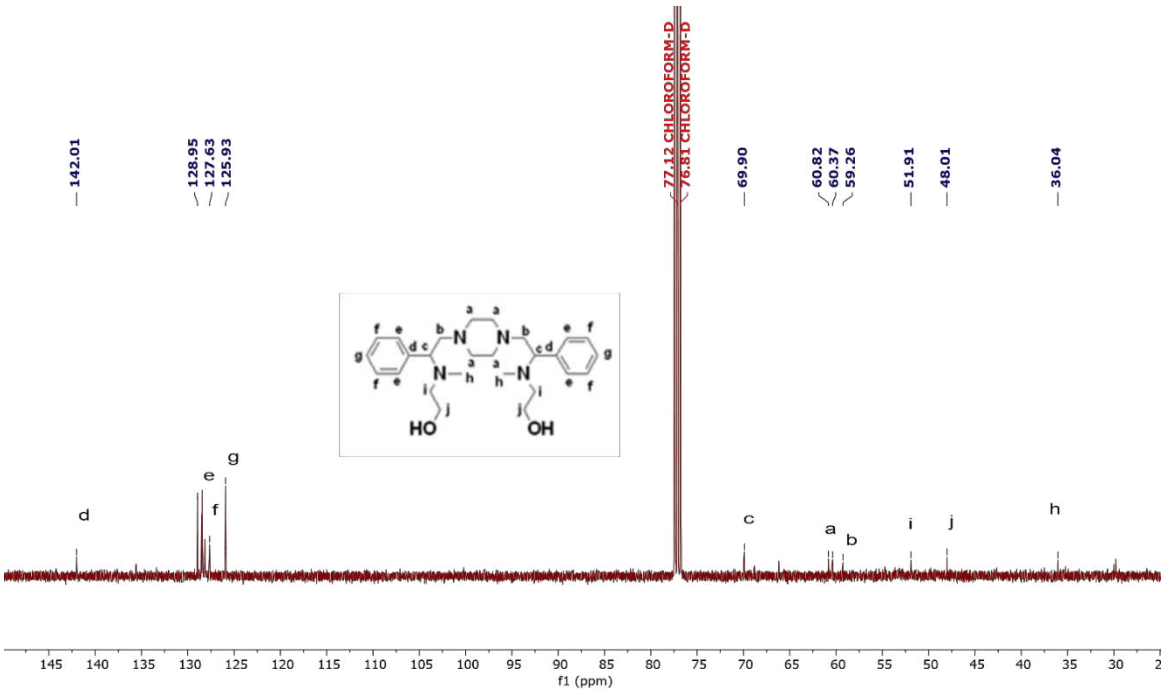


Figure 2. ^{13}C-NMR spectra of multidentate ligand (H_2L1)

3.3 Mass spectral analysis

The ligands and complexes were examined utilizing direct mass analysis in positive ionization mode. The molecular ion peak, observed at $M+H^+$ (M = molecular mass), confirms the ligand structure. Analysis of the fragmentation pattern supports structure of ligands and their metal complexes. In the mass spectra of intermediates E1, E2 and ligands H_2L1, H_2L2, molecular ion peak shows at m/z 327.19, 363.13, 441.32 and 463.32 which corresponds to the molecular mass of ligand. Detailed mass fragmentation data and their corresponding fragments for H_2L1 and Cu_2L1 are described here in while that of other complexes are described in supplementary file (figure S17-S24). In H_2L1, molecular ion peak at m/z 441.32 [$M+H^+$] corresponds to the molecular mass of ligand and molecular ion peak at m/z 471.27 [$M+K^+$] corresponds to the

molecular mass of ligand with potassium ion. In the first pathway, loss of OH-CH_2- with addition of proton represents the peaks m/z at 411.3. Further loss of CH_3-N-CH_2 with addition of 3 proton represents the peaks m/z at 381.26 and peak m/z 308.23 represent the addition of proton and loss of CH_3-N-CH_2-CH_2-OH. Continued loss of -CH_2-CH-CH_2- and benzene ring with the addition in the last fragment shows at mass m/z 204. Loss of half fragment from the ligand i.e. CH_3-N-CH_2-CH_2-OH shows at mass m/z 291 and further addition of proton and loss of -CH- and -OH appear at m/z 261.23. Peak at m/z 120.92 appear by the addition of two proton and loss of piperazine ring, -CH_2- and -CH_2-CH_2- fragment. The observed fragmentation (figure 3) pattern provides strong evidence supporting the proposed structure of the ligand.

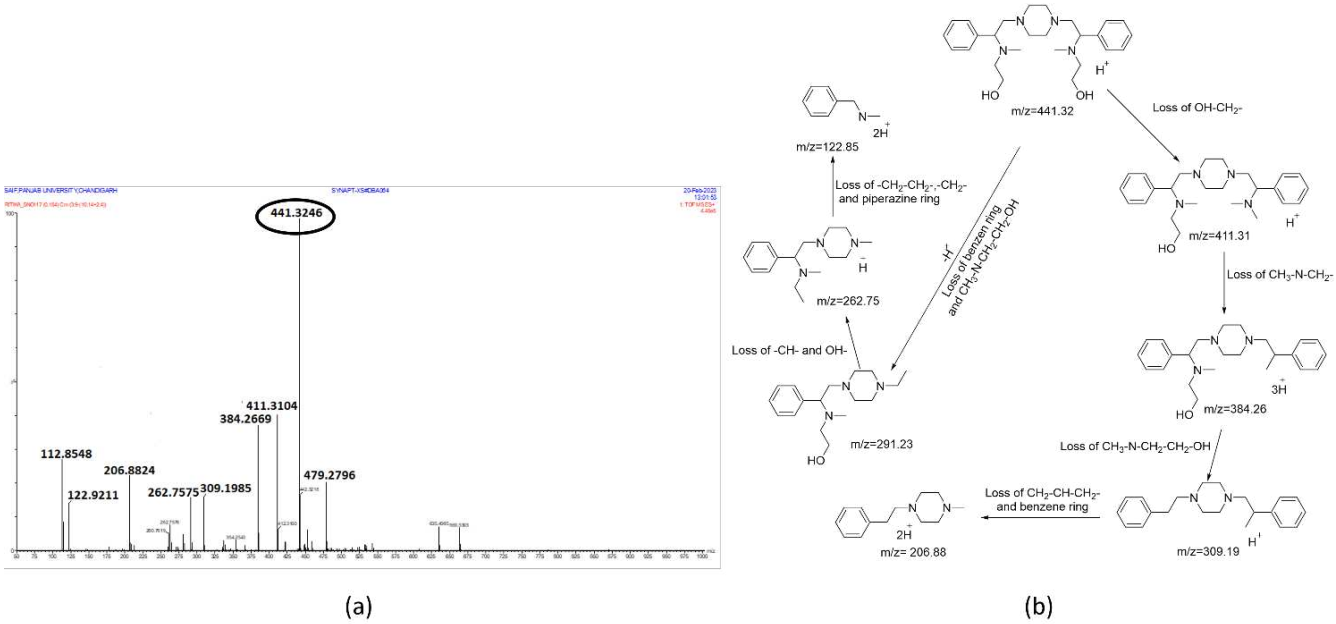


Figure 3. (a) Mass spectra of ligand H_2L1 (b) Mass fragmentation pattern of ligand H_2L1

In the mass spectra of Cu_2L1, molecular ion peak at m/z 710 corresponds to the molecular mass of the complex with K^+ ion. In the first pathway, loss of two H_2O molecules appears at peaks m/z at 634.41. Loss of Cu ion, water molecule and Cl from the complex shows peak at m/z at 558.48. Further loss of O-CH_2-CH_2-N-CH_3 from the intermediate species show peak at m/z 481.55. While peak at m/z 336.69 appear by the loss Cu ion, aqua ligand, chloro ligand and O-CH_2- give free ligand. Further loss of benzene ring from the free ligand shown peak at m/z 260.76. The observed fragmentation pattern shown in the figure 4 provides strong evidence supporting the proposed complex structure.

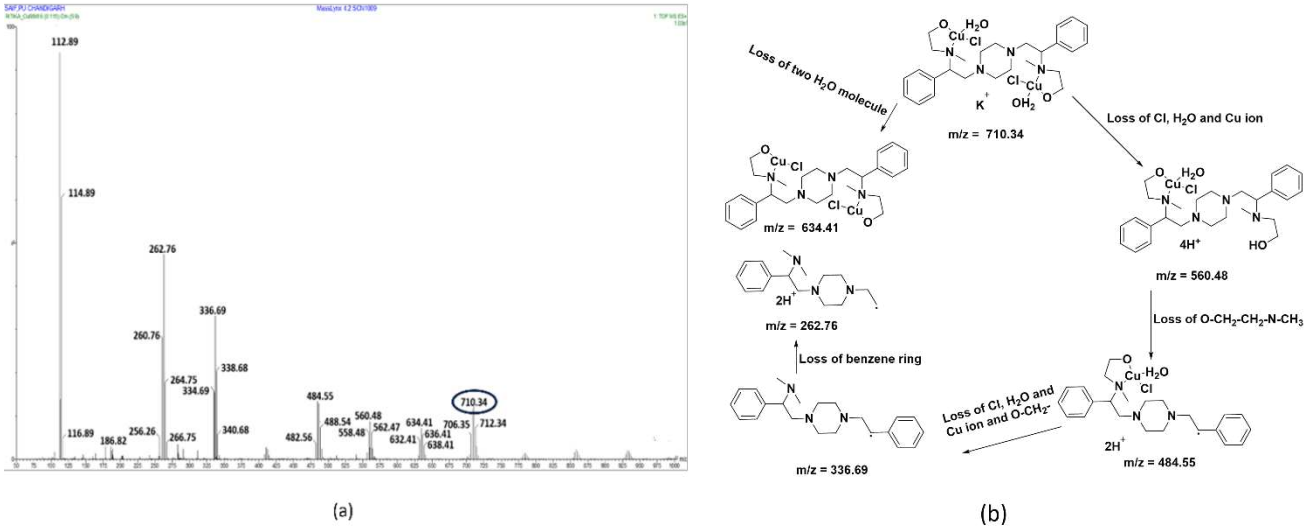
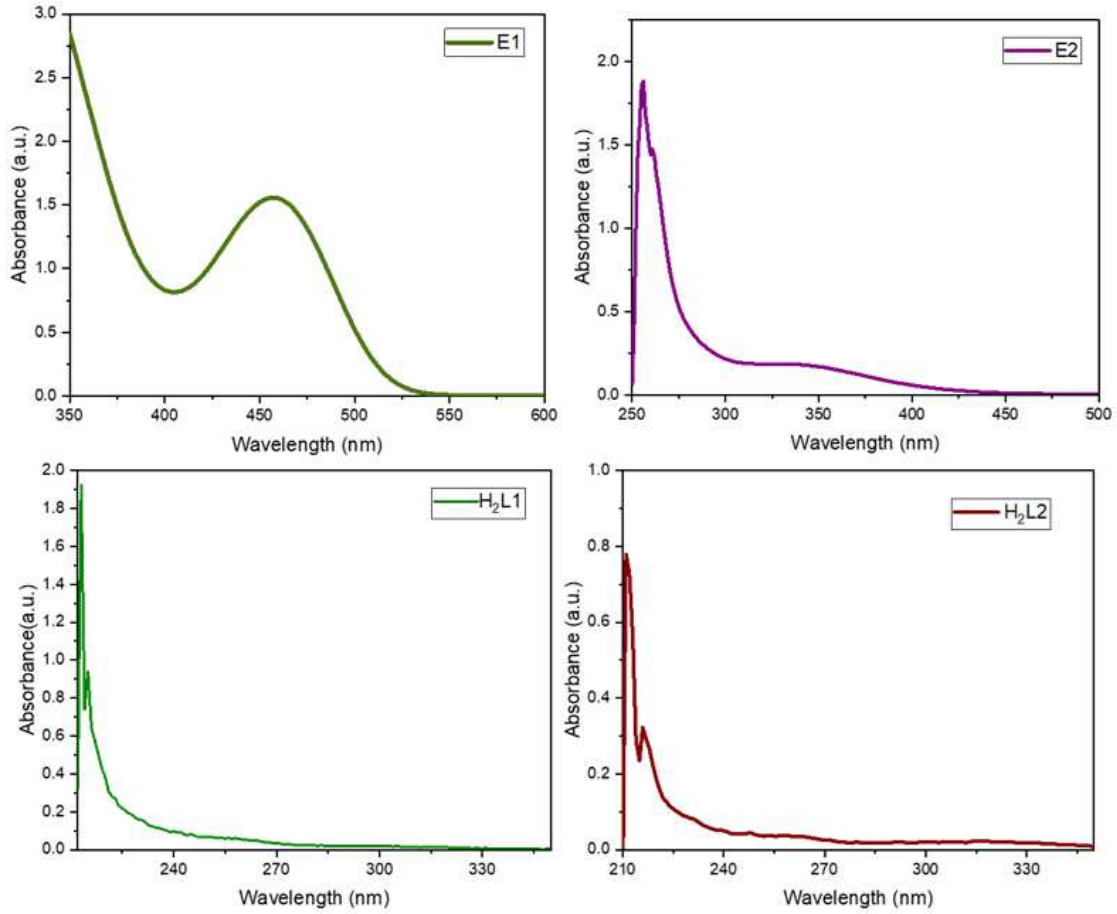


Figure 4. (a) Mass spectra of complex Cu_2L1 (b) Fragmentation pattern of complex Cu_2L1

3.4 UV-visible spectral analysis

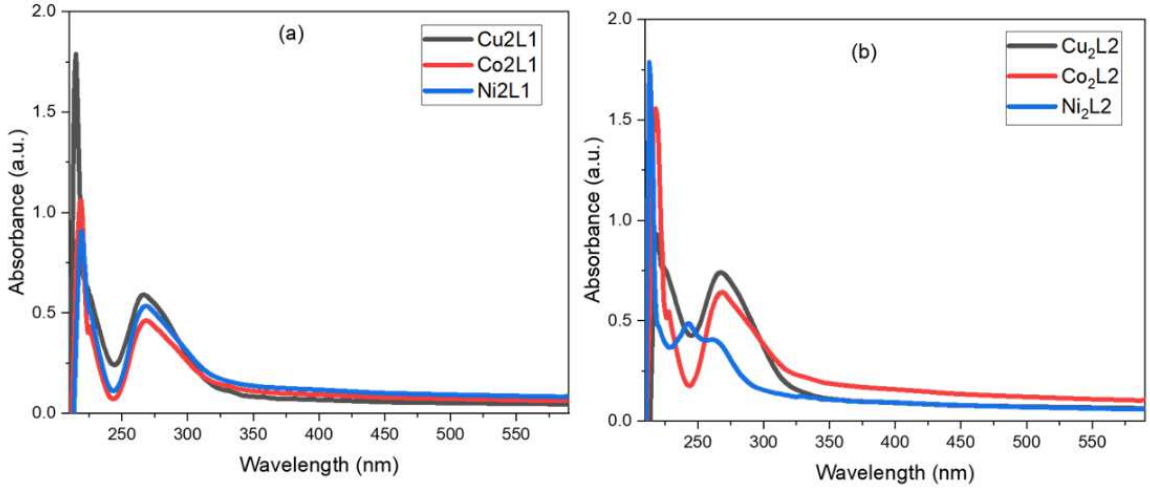
The electronic absorption spectra of the ligands and the metal complexes were recorded in methanol and acetonitrile, respectively. Since all the synthesized ligands contain aromatic moieties, characteristic electronic transitions were observed in their UV–Visible spectra. The intermediate ligands E1 and E2 exhibited absorption bands at 458 and 256 nm with molar extinction coefficients of 1.87×10^3 and 2.25×10^3 L mol^{-1} cm^{-1}, respectively, which may be attributed to π→π* and n→π* electronic transitions within the aromatic framework. The multidentate ligands H_2L_1 and H_2L_2 displayed absorption bands at 215 and 216 nm with molar extinction coefficients of 1.88×10^3 and 1.00×10^3 L mol^{-1} cm^{-1}, respectively, corresponding predominantly to ligand-centered π→π* transitions. The UV-Visible spectra of all complexes are shown in figure 6. in the absorption maxima of the metal complexes relative to the free ligands indicates successful coordination of the ligands with the metal ion. The bands observed at the range of 240- 290 nm in spectra of all complexes are assigned to π→π* transitions i.e. intra ligand charge transfer. The copper complexes Cu_2L1, Cu_2L2 showed absorbed band at 267 nm and 266 nm with the molar extinction coefficient of $0.82x10^3$ L mol^{-1} cm^{-1} and $1.48x10^3$ L mol^{-1} cm^{-1}. The cobalt complexes Co_2L1, Co_2L2 showed absorbed band at 270 nm and 268 nm with the molar extinction coefficient of $0.9x10^3$ L mol^{-1} cm^{-1} and $1.26x10^3$ L mol^{-1} cm^{-1} while the nickel complexes Ni_2L1 showed absorbed band at 268 nm and Ni_2L2 at 245 nm, 263 nm with the molar extinction coefficient of $1.06x10^3$ L mol^{-1} cm^{-1} and $0.96x10^3$ L

342 mol^{-1} cm^{-1}, $0.8x10^3$ L mol^{-1} cm^{-1} respectively [Pait et al., 2014]. The proposed electronic
343 transitions in the ligands and complexes are shown in the table 2.



344

345 **Figure 5.** UV-Visible spectra of intermediates E1, E2 and ligand H_2L1 and H_2L2



346 .

347 **Figure 6.** (a) UV-Visible spectra of binuclear complexes of H_2L1 (b) UV-Visible spectra of
348 binuclear complexes of H_2L2

Table 2. UV-Vis Absorption data of ligands and complexes

Sr. No.	Sample Code	Absorption Max.	Type of Transition	Molar extinction coefficient
1	E1	458	π→π*	$1.87x10^3$
2	E2	256	n→π*	$2.25\ x10^3$
3	H_2L1	215	n→π*	$1.88x10^3$
4	H_2L2	216	n→π*	$1x10^3$
5	Cu_2L1	267	π →π*	$0.82x10^3$
6	Co_2L1	270	π →π*	$0.9x10^3$
7	Ni_2L1	268	π →π*	$1.06x10^3$
8	Cu_2L2	266	π →π*	$1.48x10^3$
9	Co_2L2	268	π →π*	$1.26x10^3$
10	Ni_2L2	245, 263	n→π*, π →π*	$0.96x10^3$, $0.8x10^3$

3.5 Thermogravimetric analysis

Thermogravimetric analysis (TGA) was used to study the thermal stability of the complexes and to check the presence of any coordinated or solvent molecules. The TG data help to determine the temperature at which the complex starts to decompose and provide information about the overall thermal stability of the metal complex [Bouzerafa et al., 2016]. In all complexes, the initial mass loss below about 80-150 °C are attributed to the removal of lattice water or solvent (figure 7 and figure S25). Further, a major decomposition appearing between about 250 - 400°C, corresponding to the degradation of the metal complexes. The gradual decrease in mass up to 600°C are consistent towards the formation of the respective metal oxides (CuO, CoO and NiO) as final products [Sanjurani et al., 2025].

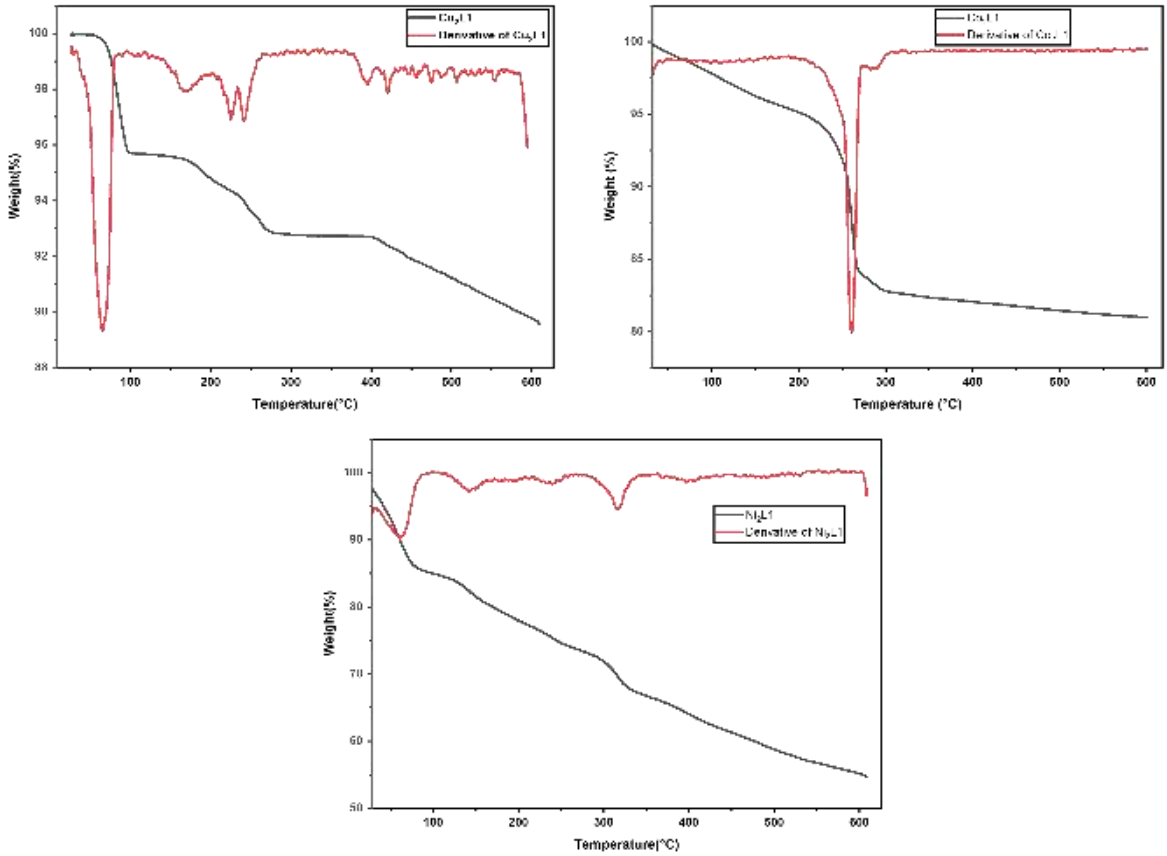


Figure 7. TGA analysis of binuclear complexes of H_2L1

3.6 EPR spectra analysis

X-band EPR spectra of the complex Cu_2L1 and Cu_2L2 were recorded with EPR spectrometer 9.48 GHz X-band microwave frequency and shown in the supplementary file figure S26. EPR spectra of both complexes were recorded at 100 K, and the obtained g-value of both complexes (Cu_2L1 and Cu_2L2) are g = 2.16 and g = 2.2 calculated by using formula (g=hν/BH) from the magnetic field along with microwave frequency. Both spectra exhibit features characteristic of S=1 Cu(II) ions in anisotropic ligand environments through ferromagnetic exchange between the two copper centres and zero field splitting of the ground triplet state [Khadir et al., 2015].

3.8 **Cytotoxic studies**

The cytotoxic potential of synthesized metal complexes (Cu_2L1, Co_2L1, Ni_2L1, Cu_2L2, Co_2L2, Ni_2L2) was assessed in BHK-21 normal cells and MCF-7 breast cancer cells using the MTT assay [Rupesh et al., 2006; Abbas et al., 2021] (figure 8). In BHK-21 cells, untreated control

cells exhibited 100% viability, and vehicle controls showed no significant effect. All metal complexes showed a dose-dependent decrease in viability, but importantly, cells maintained >60% viability even at the highest concentration (100 µg/mL). At lower concentrations (6.25 µg/mL), viability was highest for Ni_2L1 (95.11 ± 0.31%) and Co_2L1 (94.1 ± 0.28%), and lowest for Co_2L2 (85.29 ± 0.27%). Increasing the dose to 50-100 µg/mL caused a further decline in cell viability, with Co_2L2 showing the least (71.46 ± 0.26%). These results indicate that the compounds are moderately cytotoxic toward normal cells but largely well-tolerated, which is consistent with previous reports showing that metal complexes generally exhibit low toxicity toward normal cell lines. The IC_{50} values for all compounds in both BHK-21 and MCF-7 cells are summarized in Table 3. The calculated selectivity index (SI) values indicated preferential cytotoxicity of the synthesized complexes toward MCF-7 cancer cells compared to BHK-21 normal cells, with Co_2L_1 and Ni_2L_1 exhibiting particularly high selectivity. SI=

In MCF-7 cancer cells, vehicle controls again had no significant effect. All compounds displayed marked, dose-dependent cytotoxicity, reflecting anticancer activity. At 6.25 µg/mL, cell viability ranged from 55.97 ± 0.21% for Co_2L1 to 72.39 ± 0.65% for Cu_2L1, and decreased progressively with increasing concentrations. At 100 µg/mL, viability was reduced to between 35.41 ± 0.46% for Co_2L1 and 43.46 ± 0.44% for Ni_2L2, while doxorubicin, used as a reference, exhibited similar dose-dependent cytotoxicity with 11.34 ± 0.53% viability. All treated groups showed highly significant reductions compared to untreated controls ($p < 0.001$). These observations are in line with prior studies demonstrating that metal complexes exert cytotoxicity against cancer cells, including MCF-7, while sparing normal cells [Balakrishnan et al., 2020]. Overall, our findings suggest that the metal complexes exhibit cytotoxicity, effectively inhibiting MCF-7 cancer cells while maintaining moderate viability in BHK-21 normal cells, highlighting their therapeutic potential with minimal toxicity to normal cells. Comparison study of cytotoxic study synthesized compounds with published compounds shown in table 4.

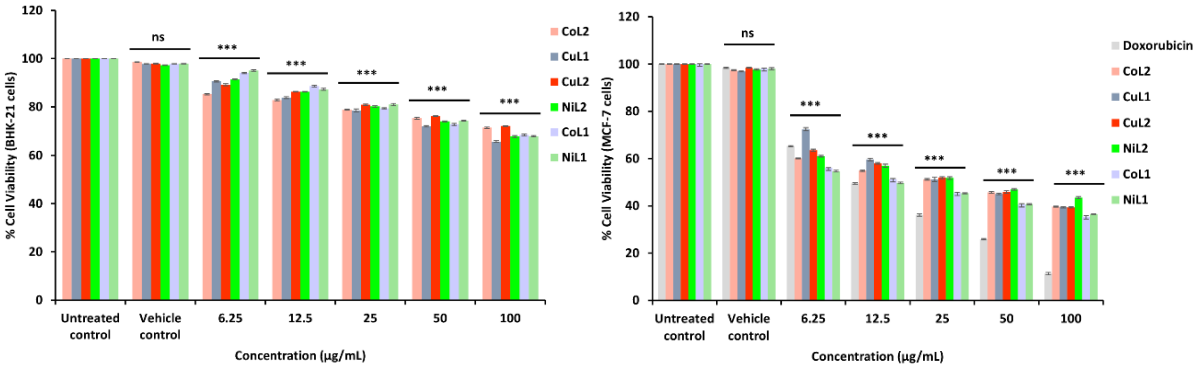
Table 3. Half-maximal inhibitory concentration (IC_{50}) values of doxorubicin and synthesized metal complexes on normal (BHK-21) and breast cancer (MCF-7) cell lines determined by the MTT assay. Values are expressed as IC_{50} in µg/mL (Mean ± SD, n = 3).

Compounds	Doxorubicin	Cu_2L1	Co_2L1	Ni_2L1	Cu_2L2	Co_2L2	Ni_2L2

IC_{50} (µg/mL)	BHK-21	-	156.1	159.2	159.5	217.4	245.6	167.1
	MCF-7	14.18	50.70	17.26	12.34	46.10	40.24	50.60
Selectivity Index (SI)	IC_{50} (MCF-7)/IC_{50} (BHK-21)	-	3.07	9.22	12.90	4.71	6.10	3.30

404

405



406

407 **Figure 8.** Effect of metal complexes on the viability of (a) BHK-21 cells and (b) MCF-7 cells
408 at various concentrations. Data are presented as mean ± SD of three independent experiments
409 (n = 3). Statistical significance compared with untreated control: ns = not significant, ***p <
410 0.001.

411 **Table 4.** Comparison study of cytotoxic study synthesized compounds with published
412 compounds.

Compounds	MCF-7	Reference
Cu_2L'	6.01	[Kant and Maji, 2023]
Cu_2L''	8.95	[Kant and Maji, 2023]
Cu_2L'''	5.06	[Kant and Maji, 2023]
$[Cu_2(pza)_2(2\text{-methoxybenzoate})_4]$	64.98	[Ahmad et al., 2021]
$[Cu_2(pza)_2(3\text{-methoxybenzoate})_4]$	85.54	[Ahmad et al., 2021]
C1	204.25	[Iacopetta et al., 2021]

C2	196.56	[Iacopetta et al., 2021]
C3	248.58	[Iacopetta et al., 2021]
C4	73.05	[Iacopetta et al., 2021]
Cu_2L1	50.70	This work
Co_2L1	17.26	This work
Ni_2L1	12.34	This work
Cu_2L2	46.10	This work
Co_2L2	40.24	This work
Ni_2L2	50.60	This work

3.9 Antibacterial Assays

In antimicrobial assays, the free ligands exhibited minimal activity, whereas the metal complexes demonstrated moderate to high activity compared with the standard drug amikacin. The enhanced activity of the metal complexes relative to the ligands may be attributed to increased hydrophobicity upon chelation, which reduces the polarity of the metal ion through partial charge sharing with donor atoms and facilitates penetration through microbial cell membranes. This alteration in polarity likely enhances the ability of the complexes to traverse lipid layers, thereby improving antimicrobial efficacy. The antibacterial activity of synthesized compounds and comparison study with published compounds are shown in table 5. The antibacterial results indicated that the complexes were generally more active against both *E. coli* and *S. aureus* than the corresponding free multidentate ligands (figure 9 (a)). For *S. aureus*, significant differences were observed between amikacin and several compounds. Complexes Cu_2L2, Co_2L2 and Ni_2L2 showed highly significant differences compared with amikacin ($p<0.001$). Ni_2L2 also differed very significantly from amikacin ($p < 0.01$). In contrast, Cu_2L1 and Co_2L1 did not show any significant when compared to amikacin (ns), indicating comparable antibacterial activity against *S. aureus*. In the case of *E. coli*, most complexes showed highly significant differences relative to amikacin (figure 9 (b)). Cu_2L2, Co_2L2, Ni_2L2, Cu_2L1, and Ni_2L1 demonstrated highly significant differences ($p < 0.001$), while Co_2L1 also showed the significant difference ($p<0.01$). These findings indicate that metal chelation markedly enhances antibacterial activity, particularly against *E. coli*. The polarity of the metal

ion is reduced by chelation of complexes, mainly by a partial sharing of its positive charge with these donor groups and possibly by the displacement of the p-electrons in the whole chelate ring system [Asbahy et al., 2016]. Consequently, this chelation process enhances the lipophilic properties of the central metal atom and facilitates its passage through the lipid layer. This allows the metal complex to cross the cell wall membrane of the micro-organism more efficiently, increasing the activity of the drug [Priya et al., 2025].

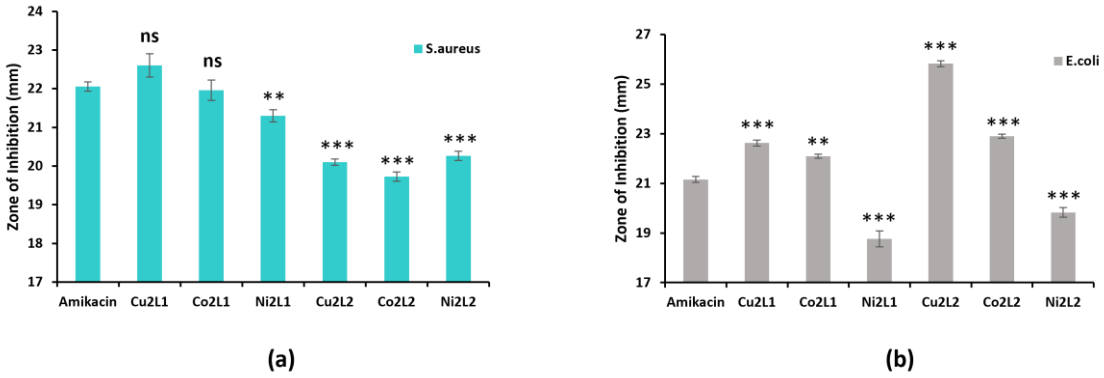


Figure 9. Effect of metal complexes against standard drug (a) *S. aureus* and (b) *E. coli.* Data are presented as mean ± SD of three independent experiments (n = 3). Statistical significance compared with untreated control: ns = not significant, ***p < 0.001.

Table 5. Comparison of Antibacterial activities of reported compounds with synthesized ligands and complexes.

Sample Code	Average Inhibition Zone in diameter (mm) ± SD		Reference
	E. coli	*S. aureus*	
$[Cu_2(pza)_2(2\text{-methoxybenzoate})_4]$	125	125	[Ahmad et al., 2021]
$[Cu_2(pza)_2(3\text{-methoxybenzoate})_4]$	125	125	[Ahmad et al., 2021]
BMB-Cu	16	18	[Babu and Pitchai, 2014]
BMB-Co	8	14	[Babu and Pitchai, 2014]
BMB-Ni	10	-	[Babu and Pitchai, 2014]
Cu_2L	26	25	[Chohan et al., 2002]
Co_2L	22	23	[Chohan et al., 2002]

Ni_2L	21	23	[Chohan et al., 2002]
$[Cu(L1)phen]Cl_2$	18	28.50	[Nishat et al., 2007]
$[Cu(L1)bpy]Cl_2$	-	17.66	[Nishat et al., 2007]
$[Cu(L2)phen]Cl_2$	22	30.40	[Nishat et al., 2007]
$[Cu(L1)bpy]Cl_2$	14	15.33	[Nishat et al., 2007]
H_2L1	-	-	This work
Cu_2L1	22.6+0.12	22.6+0.3	This work
Co_2L1	22.1+0.08	21.9+0.26	This work
Ni_2L1	18.7+0.32	21.3+0.16	This work
H_2L2	-	-	This work
Cu_2L2	25.8+0.12	20.1+0.08	This work
Co_2L2	22.9+0.08	19.7+0.12	This work
Ni_2L2	19.8+0.2	19.8+0.2	This work
Amikacin	21.16+0.12	22.06+0.12	This work
DMSO	Nil	Nil	This work

3.10 BSA Binding Studies

Serum albumins (SA), like human serum albumin (HSA), play a pivotal role in the physiological transport of a wide range of endogenous and exogenous compounds, including metals ions and metal-based drugs, through the bloodstream to target cells and tissues. They serve as significant mediator for drug pharmacokinetics and bioavailability due to their extensive binding ability and compatibility with a variety of ligands. Bovine serum albumin (BSA) is the most extensively studied serum albumin because of its high structural homology with HSA (human serum album) [Aggarwal et al., 2020]. In this study, binding interactions between synthesized metal complexes and BSA were investigated using UV-Vis absorption spectroscopy. A 0.1 M Tris buffer was employed for all spectroscopic measurements. Solutions of BSA (1 mM) and metal complexes (50 μM) were prepared, and absorption spectra were recorded both in the presence and absence of BSA. The absorption spectra of complexes (Cu2L1 and Co_2L2) were recorded with the presence and absence of BSA as shown in figure 10. Binding interactions were assessed through a titration method in which the concentration of BSA was varied with respect to fixed concentration of the metal complex in the array of 0-3μM. The absorption spectra of other complexes (Co_2L1, Ni_2L1, Cu_2L2 and Ni_2L2) was

recorded with the presence and absence of BSA as shown in supplementary file figure S28-S31. Binding interactions were assessed through a titration method in which the concentration of BSA was varied with respect to fixed concentration of the metal complex in the array of 0-3µM. As shown in figure 6., BSA shows absorbance at 273 nm in spectra, with increase in the concentration of BSA significant a red shift which suggest interaction of BSA with metal complex [Tan et al., 2008]. A direct proportional relationship appears between the band's intensity and the BSA concentration. Their binding constants were then determined by calculations were performed using a double reciprocal plot of 1/[BSA] versus $1/(A - A_0)$, following previously established methods. The binding affinity of the complexes toward BSA was quantitatively assessed using a double reciprocal method based on the modified Benesi-Hildebrand equation:

$$\Delta A/b=(S_t K_{11} \Delta\epsilon_{11}[L])/(1+K_{11}[L]) \quad \text{---------(1)}$$

Where, $\Delta A = A - A_0$, is the difference in absorbance,

A: absorption signal at variant complex - [BSA] concentrations,

b is the path length of the cuvette,

S_t is the total concentration of the substrate (metal complex),

K_{11} is the binding constant,

$\Delta\varepsilon_{11}$ signifies molar absorptivity of BSA - metal complex,

[L] is the concentration of free BSA.

$$\text{Where, } \Delta\varepsilon_{11} = \varepsilon_{11} - \varepsilon S - \varepsilon L \quad \text{----------(2)}$$

Where, εS signifies molar absorptivity of unbound metal complex,

εL signifies molar absorptivity of the BSA.

Therefore, double reciprocal plot of $1/(A-A_0)$ vs. 1/ [BSA] comes out to be linear and the values of binding constant (K_b in M^{-1}) can be calculated as: Linear fit curves are utilized to determine the binding constants and shown in table 6. Binding constant value indicated moderate binding of complexes with BSA protein, which favoured serum protein's role as a transporter for drug delivery [Nafisi and Bagheri Sadeghi, 2011; Jovanović et al., 2016]. The

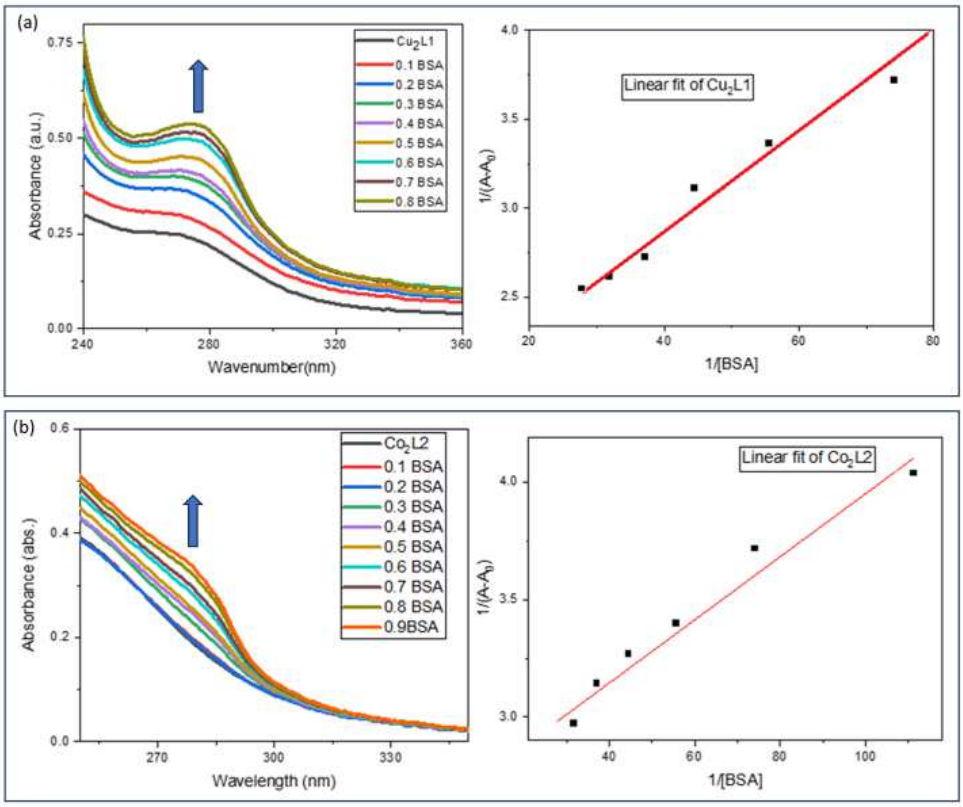
linearity of these plots indicated a single binding site model and facilitated the determination of binding constants.

$$K_b = \text{intercept/slope} \qquad \text{--------(3)}$$

As shown in table 6, dinickel complexes show less binding with BSA as compare to dicopper complexes and dicobalt complexes. Overall, the moderate to strong binding behaviour of the synthesized complexes with BSA supports their viability as potential metal-based anticancer drug candidates, capable of effective serum transport. Overall, the trend in BSA binding affinities follows the order: $Cu_2L2 \approx Co_2L2 > Cu_2L1 > Co_2L1 >> Ni_2L2 \approx Ni_2L1$, indicating that both the metal ion and ligand architecture significantly influence the extent of protein interaction. Further, interaction of complexes with BSA had been validated through molecular docking studies which provide deeper insights into specific binding residues [Kratz, 2008; Karthikeyan et al., 2015].

Table 6. Binding constant value (K_b M^{-1}) of complexes with BSA.

Sample Code	Binding constant values (K_b M^{-1})
Cu_2L1	117.11
Co_2L1	104.78
Ni_2L1	10.63
Cu_2L2	198.77
Co_2L2	194.21
Ni_2L2	11.41



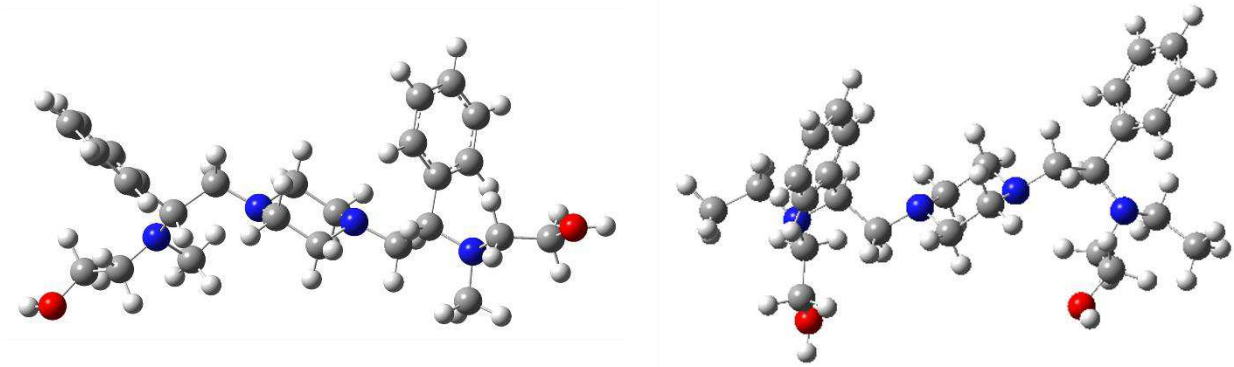
507

508 **Figure 10.** (a) UV-vis spectra of titration curves of complex Cu_2L1 with increasing BSA
509 concentration in the range 0-3 μM, along with Linear fit of $1/(A-A_0)$ vs 1/[BSA]. (b) UV-vis
510 spectra of titration curves of complex Co_2L2 with increasing BSA concentration in the range
511 0-3 μM along with Linear fit of $1/(A-A_0)$ vs 1/[BSA].

512 **3.11 Geometry Optimization Studies**

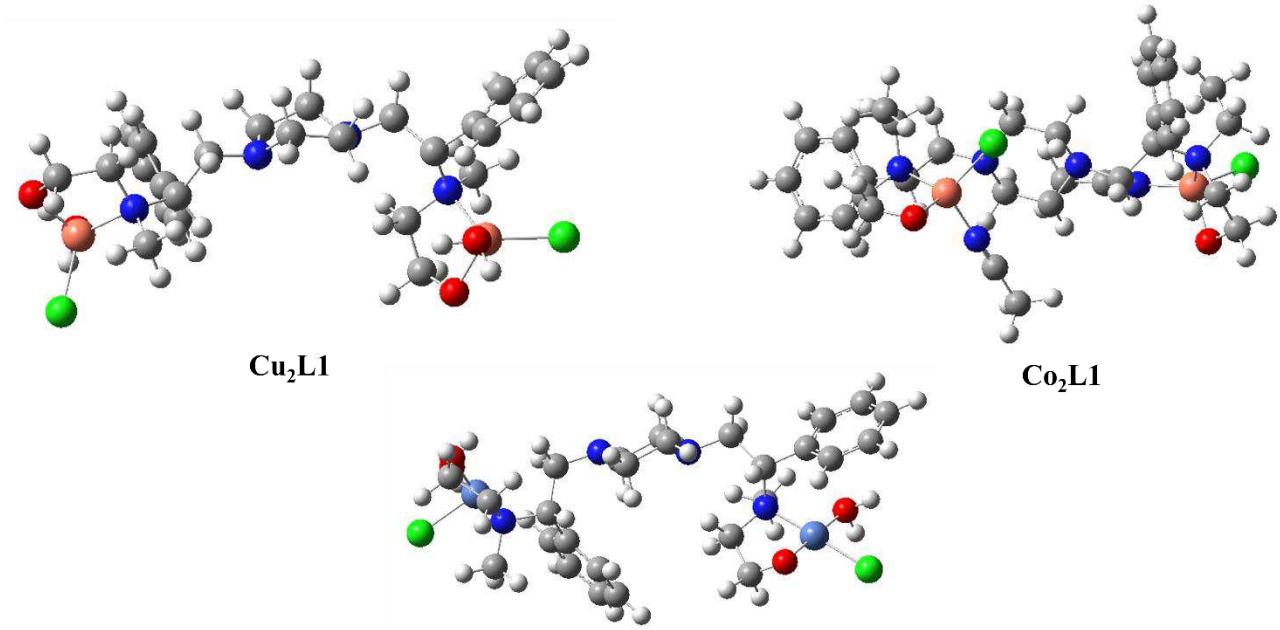
513 Geometry optimization was performed to obtain the most stable molecular conformations and
514 energetically favourable geometries of the ligands and metal complexes. Geometry
515 optimization ensures that the molecule structure closely resembles the true molecular
516 conformation under realistic conditions. Energy minimization plays a key role in identifying
517 the most stable forms of molecules by exploring various conformations and selecting those
518 corresponding to local or global energy minima. This method is usually done through quantum
519 mechanics and it allows scientists to obtain predictions of the low-energy structures through
520 the potential energy surface. The low-energy structures are particularly helpful when applied
521 in coordination chemistry since they provide information regarding how the donor atoms are
522 orientated for bonding purposes with metals. In this study, the ligands H_2L1 and H_2L2 were

optimized using Gaussian 09, applying the hybrid functional method B3LYP along with the 6-31G(2d,2p) basis set. For the metal complexes, geometry optimization was done using semi empirical, method PM6 [Elabdeen et al., 2021]. Although the PM6 method is not favoured for the description of noncovalent interactions, still it was preferred here due to the lower computational cost. Although Density Functional Theory (DFT) is more accurate and robust for calculating many properties, the significant computational load, it's inherent difficulty in predicting correlated system and problems in defining spin state are some of its drawbacks. This makes PM6 as a viable option for complexes with multiple metal centers with partially filled d-orbitals. The optimized structure of ligands and complexes shown in figure 11.



H_2L1 H_2L2

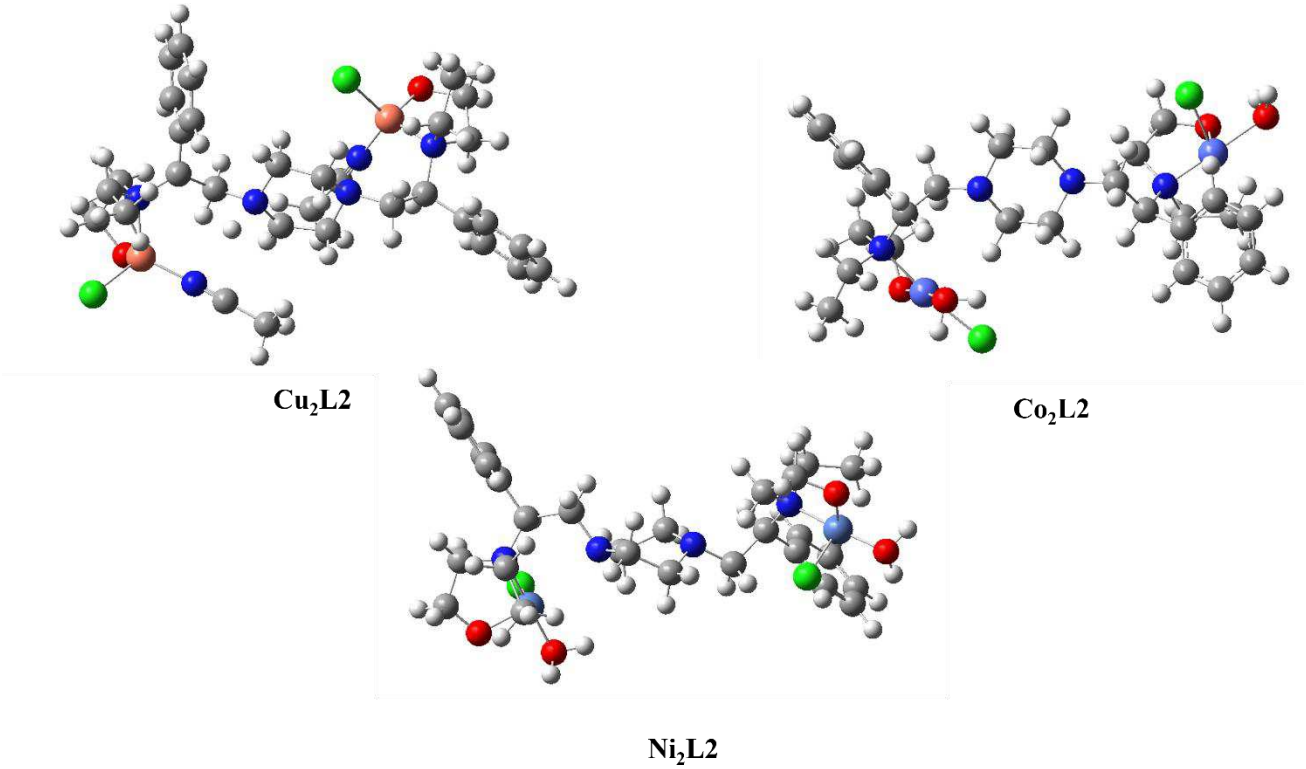
(a) Optimized structure of multidentate ligands



Cu_2L1 **Co_2L1**

Ni_2L1

(b) Optimized complexes structure of H_2L1



(c) Optimized complexes structure of H_2L2

Figure 11. Optimization structure of compounds. (a) Optimized structure of multidentate ligands. (b) Optimized complexes structure of H_2L1. (c) Optimized complexes structure of H_2L2.

3.12 Frontier Molecular Orbital (FMO) study

Frontier molecular orbital (FMO) analysis provides valuable insight into the reactivity and stability of the synthesized ligands and their metal complexes. From the computed HOMO and LUMO energy levels, it is evident how effective the compounds could be in donating and accepting electrons. The difference in energy between HOMO and LUMO levels, denoted by ΔE, is an important parameter used in predicting the stability, reactivity, and other properties related to light absorption by the compounds. In the present investigation, the energy gap (ΔE) for the ligands was relatively high implying their high kinetic stability and low reactivity. However, after complexation with the transition metal elements, there was significant decrease in ΔE energy value as shown in figure 12; the complexes of Cu (II) and Ni (II) had the lowest ΔE values. This suggests increased charge transfer ability and chemical softness in the

complexes due to their increased polarization and efficiency in interacting with biological systems [Kant et al., 2022].

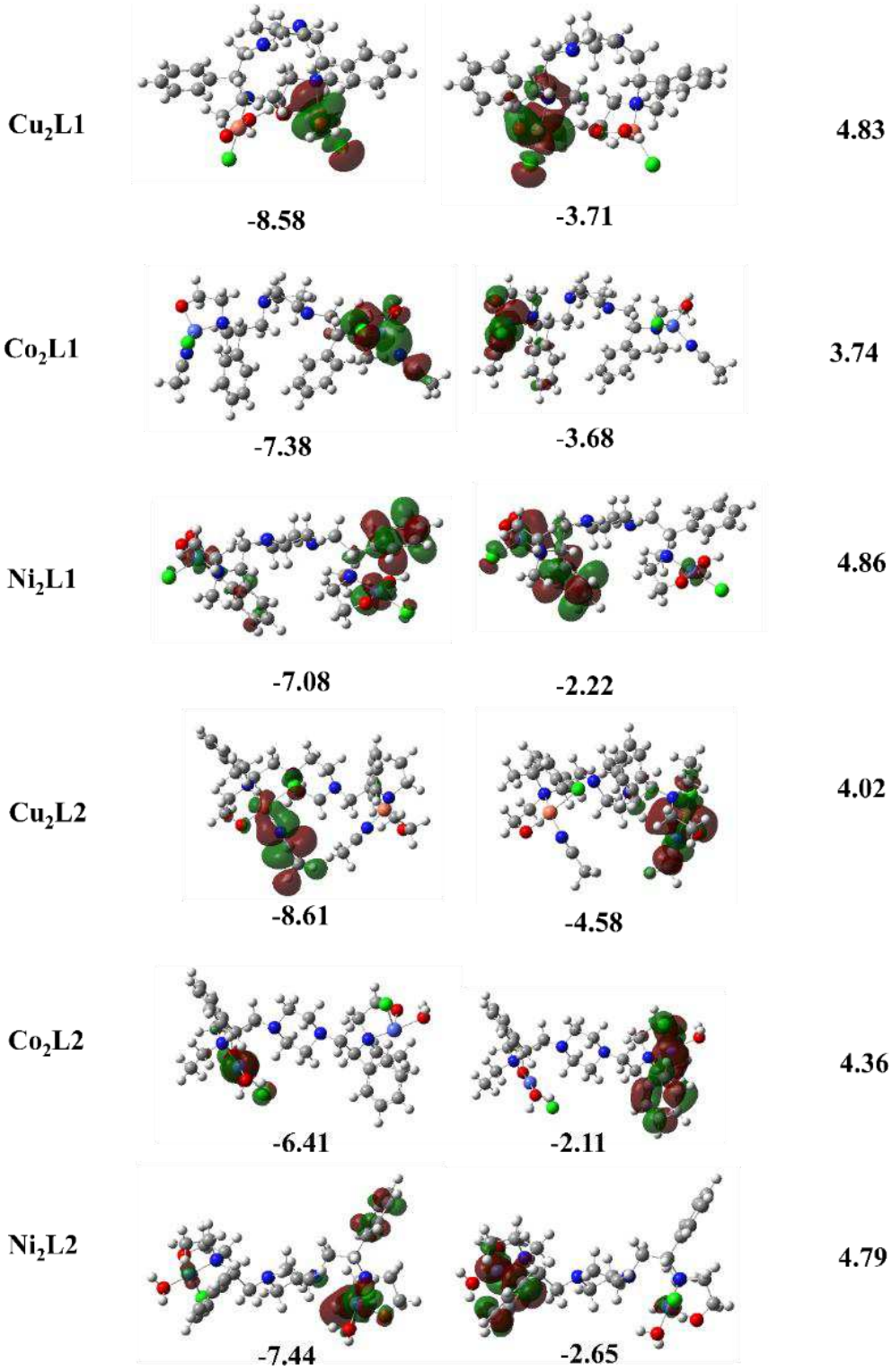


Figure 12. Frontier molecular orbital (FMO) diagrams of binuclear complexes of H_2L1 and H_2L2 showing the spatial distribution of the HOMO and LUMO orbitals along with their corresponding energy values and energy gaps in eV.

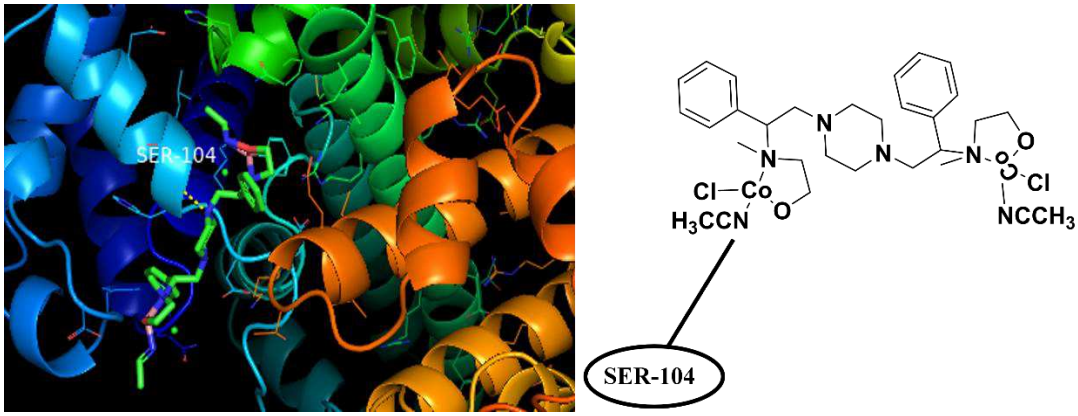
3.13 Molecular Electrostatic Potential (MEP) study

Molecular Electrostatic Potential (MEP) map studies have been carried out to gain insights into the electronic structure, possible reactive sites, and the impact of metal coordination to the ligands. Red, blue, and green-yellow indicate regions of higher negative (electrons-rich), higher positive (electron-deficient), and intermediate potentials respectively on the MEP maps of the molecules. The regions with highest red MEP in free ligands are around the oxygen and nitrogen atoms of the ligands indicating the highly electron-rich nature of these regions. These are therefore the most probable nucleophilic sites of the ligand. The blue MEP in vicinity of the hydrogen atoms shows localization of positive charges suggesting weak electrophilicity. Upon coordination with Cu(II), Co(II), and Ni(II) ions, the MEP maps figure S32 show significant shifts in electron distributions. The reduction in the intensities of the red MEP near the donor sites is an indication of electrons donation from O/N atoms to the metal ion. Additionally, there are distinct blue regions formed around the metal ion, showing accumulation of positive charge on the metal ions and electrophilic nature. Among the complexes, the Cu(II) complex displays the strongest positive potential around the metal center, indicating higher charge polarization and stronger metal–ligand interaction. The Co(II) complex shows moderately distributed potential, while the Ni(II) complex exhibits the most uniform green–blue distribution, suggesting increased charge delocalization and comparatively greater electronic stabilization [Chen et al., 2016].

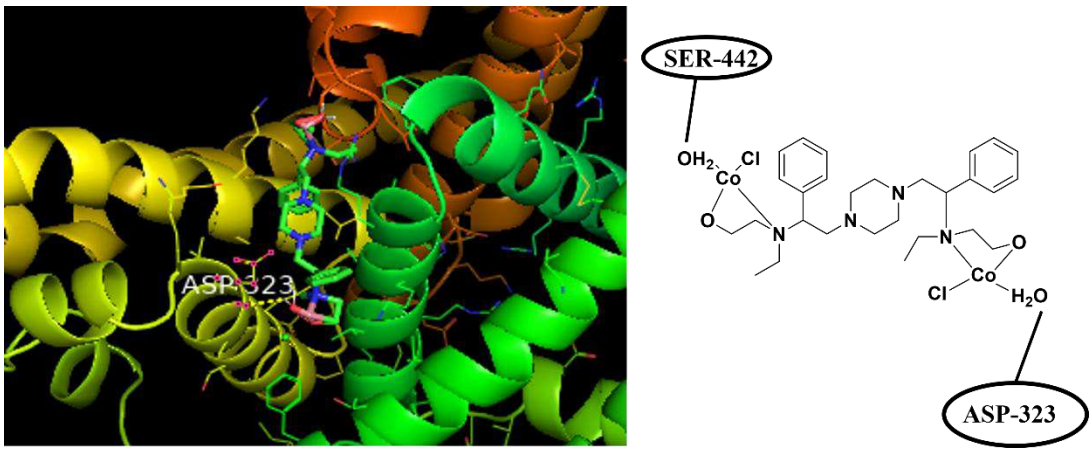
3.14 Molecular Docking

Molecular docking of complexes has been performed in order to check the available binding interaction with the BSA protein. This theoretical interaction provides insights for mechanistic interaction of these complexes with the protein and thereby providing a significant information about availability of binding sites. Molecular docking was performed using Autodock 1.5.7 tool and Autodock vina and were visualised using PyMol [Uzun et al., 2019]. BSA Protein (3v03) and reference ligand (4OR0) were downloaded from Protein Data Bank (PDB). All other necessary steps required in performing the docking has been followed from the published

literature. Water molecules are removed from the target molecule and the Kollamn united atom charges applied. All missing hydrogens were added using Autodock 1.5.7 tool. Naproxen ligand with BSA showed -6.9 binding affinity having polar contacts with SER-428 and LYS-217 amino acids residue in the BSA chain (figure S33). For the complexes, the minimum energy structure from the PM6 calculation was used. Docking result of Co_2L1 indicate interaction with SER-204 with -9.1 Kcal/mol while Co_2L2 indicate that binding affinity of this complex is -8.6 kcal/mol having polar contacts with ASP-323 and SER-442 amino acid residue in the BSA chain. The pictorial representation of docked pose of complex is presented along with 2D explanation in figure 13. Docking result of Cu_2L1 indicate interaction with LYS-294 and GLU-291 with -7.5 Kcal/mol while Cu_2L2 indicate that binding affinity of this complex is -7.7 kcal/mol having polar contact with ASP-107, TYP-451 amino acid residues in the BSA chain. Docking result of Ni_2L1 indicate interaction with SER-479, LEU-480 with -8.1 Kcal/mol while Ni_2L2 indicate that binding affinity of this complex is -8.8 kcal/mol having polar contacts with ARG-347 and ALA-324 amino acids residue in the BSA chain. The pictorial representation of docked pose of complex is presented along with 2D explanation in figure S33.



(a) Docking visualization of Co_2L1 with BSA Protein along with 2D explanation



(b) Docking visualization of Co_2L2 with BSA Protein along with 2D explanation

Figure 13. Docking visualization of dicobalt complex of H_2L1 and H_2L2 with BSA Protein along with 2D explanation.

4. Conclusions

Two new piperazine-based multidentate ligands and their binuclear Cu(II), Co(II), and Ni(II) complexes were successfully synthesized and comprehensively characterized. Spectroscopic investigation including FT-IR, UV-Visible, mass spectrometry, and EPR analysis provide the evidence of binding of metal ion with the ligand and the coordination environment. The binuclear character of Cu_2L1 and Cu_2L2 was further confirmed by the anisotropic EPR peaks. Biological activities revealed that metal complexation significantly enhances the antibacterial efficacy of the ligands, as demonstrated by larger zones of inhibition of Cu_2L2 against *E. coli* (25.8+0.12 mm) and Cu_2L1 against *S.aureus* (21.9+0.26 mm). In vitro cytotoxicity assays on MCF-7 breast cancer cells showed promising anti-proliferative effects, with the complexes displaying lower IC_{50} values compared to the standard (12-51), and BHK-21 normal cells showed less toxicity as compare to cancer cell line (IC_{50} value 150-250), indicating their potential as selective anticancer agents. Among the investigated complexes, Co_2L1 and Ni_2L1 exhibited particularly promising cytotoxic profiles with favorable selectivity toward cancer cells. Additionally, moderate binding constants observed in BSA binding studies (10-128 M^{-1}) and explored with molecular docking suggested favorable protein–complex interactions, indicating potential applicability in biomolecular transport and drug delivery processes. Computational investigations including FMO and MEP analyses further demonstrated enhanced electronic reactivity, charge redistribution, and favorable coordination behavior

upon metal complexation, which correlated well with the observed biological activities. Overall, the combined spectroscopic, computational, and biological findings suggest that these piperazine-based binuclear metal complexes represent promising scaffolds for the development of biologically active metallopharmaceutical agents.

Conflict of interest: Authors declare no conflict of interest

Funding: This research received no specific grant from any funding agency in the public, commercial, or not-for-profit sectors.

Acknowledgements: We are grateful to CIF, Lovely Professional University for FT-IR, IIT Ropar for NMR and PU-SAIF for MS. Supporting information for this article is given via a link at the end of the document.

References

Abbas S, Rashid F, Ulker E, Zaib S, Ayub K, Ullah S, Nadeem MA, Yousuf S, Ludwig R, Ali S, Saghir JI (2021) Anticancer evaluation of a manganese complex on HeLa and MCF-7 cancer cells: design, deterministic solvothermal synthesis approach, Hirshfeld analysis, DNA binding, intracellular reactive oxygen species production, electrochemical characterization and density functional theory. J Biomol Struct Dyn 39:1068–1081.

Aggarwal N, Kant R, Kumar G, James C, Maji S (2020) Synthesis, characterization and biological evaluation studies of Cu(II) and Zn(II) complexes with gly-o-andn or gly-p-andn as primary ligand and N,N' donors as secondary ligand. J Phys Conf Ser 1531:012111.

Ahmad MS, Khalid M, Khan MS, Shahid M, Ahmad M, Saeed H, Ashafaq M (2021) Tuning biological activity in binuclear Cu(II) complexes derived from pyrazine ligands: structure, magnetism, catecholase, antimicrobial, antibiofilm, and antibreast cancer activity. Appl Organomet Chem 35.

Alaghaz ANM, Ammar RA (2010) New dimeric cyclodiphosph(V)azane complexes of Cr(III), Co(II), Ni(II), Cu(II), and Zn(II): preparation, characterization and biological activity studies. Eur J Med Chem 45:1314–1322.

Alaghaz ANM, El Sayed BA, El-Henawy AA, Ammar RA (2013) Synthesis, spectroscopic characterization, potentiometric studies, cytotoxic studies and molecular docking studies of

655 DNA binding of transition metal complexes with 1,1-diaminopropane–Schiff base. J Mol
656 Struct 1035:83–93.

657 Asbahy WMA, Usman M, Arjmand F, Shamsi M, Tabassum S (2016) A binuclear
658 copper(II) complex with piperazine bridge ligand as a potential anticancer agent: DFT
659 computation and biological evaluation. Inorg Chim Acta 445:167–178.

660 Asif M (2015) Anti-tubercular activity of some six membered heterocycle compounds.
661 Chem Int 1:134–163.

662 Babu K, Pitchai P (2014) The new transition metal complexes of N,N'-(piperazine-1,4-
663 di(bisphenylmethylene)) diacetamide and their biological activity. Int J Pharm Chem Biol
664 Sci 4:145–151.

665 Balakrishnan N, Haribabu J, Dhanabalan AK, Swaminathan S, Sun S, Dibwe DF,
666 Bhuvanesh N, Awale S, Karvembu R (2020) Thiosemicarbazone(s)-anchored water-soluble
667 mono- and bimetallic Cu(II) complexes: enzyme-like activities, biomolecular interactions,
668 anticancer property and real-time live cytotoxicity. Dalton Trans 49:9411–9424.

669 Bhat IUH, Tabassum S (2009) Synthesis of new piperazine derived Cu(II)/Zn(II) metal
670 complexes, their DNA binding studies, electrochemistry and anti-microbial activity:
671 validation for specific recognition of Zn(II) complex to DNA helix by interaction with
672 thymine base. Spectrochim Acta A Mol Biomol Spectrosc 72:1026–1033.

673 Bhati S, Kumar V, Singh S, Singh J (2019) Synthesis, biological activities and docking
674 studies of piperazine incorporated 1,3,4-oxadiazole derivatives. J Mol Struct 1191:197–205.

675 Bouzerafa B, Ourari A, Aggoun D, Ruiz-Rosas R, Ouennoughi Y, Morallon E (2016) Novel
676 nickel(II) and manganese(III) complexes with bidentate Schiff-base ligand: synthesis,
677 spectral, thermogravimetry, electrochemical and electrocatalytical properties. Res Chem
678 Intermed 42:4839–4858.

679 Chandra S, Jain D, Sharma AK (2009) EPR, mass, electronic, IR spectroscopic and thermal
680 studies of bimetallic copper(II) complexes with tetradentate ligand, 1,4-diformyl piperazine
681 bis(carbohydrazone). Spectrochim Acta A Mol Biomol Spectrosc 71:1712–1719.

682 Chaudhary P, Kumar R, Verma AK, Singh D, Yadav V, Chhillar AK, Sharma GL, Chandra
683 R (2006) Synthesis and antimicrobial activity of N-alkyl and N-aryl piperazine derivatives.
684 Bioorg Med Chem 14:1819–1826.

685 Chen ZJ, Chen YN, Xu CN, Zhao SS, Cao QY, Qian SS, Qin J, Zhu HL (2016) Synthesis,
686 crystal structures, molecular docking, and in vitro biological activities evaluation of
687 transition metal complexes with 4-(3,4-dichlorophenyl)piperazine-1-carboxylic acid. J Mol
688 Struct 1117:293–299.

689 Chohan ZH, Pervez H, Rauf A, Supuran CT (2002) Antibacterial role of $SO4^{2-}$, $NO3^{-}$,
690 $C2O4^{2-}$ and $CH3CO2^{-}$ anions on Cu(II) and Zn(II) complexes of a thiadiazole-derived
691 pyrrolyl Schiff base. Met Based Drugs 8:263–267.

692 Das M, Ari B, Giri M, Das UK, Kundu P, Mahata R, Choudhury SM, Chakraborty A,
693 Samanta BC, Mondal S, Maity T (2025) Cu(I) and Cu(II) complexes with a piperazine-
694 containing N,N,O-chelate ligand: a combined theoretical and experimental investigation.
695 Eur J Inorg Chem 28.

696 Dong WK, Sun YX, Zhang YP, Li L, He XN, Tang XL (2009) Synthesis, crystal structure,
697 and properties of supramolecular Cu(II), Zn(II), and Cd(II) complexes with Salen-type
698 bisoxime ligands. Inorg Chim Acta 362:117–124.

699 Elabdeen AZ, Saleem WM, El-Tahawy MMT, Ali AE (2021) Theoretical, experimental
700 investigations and computational molecular modeling of amoxicillin metal complexes.
701 Chem Res J 6:26–54.

702 Gokturk T, Cetin ES, Hokelek T, Pekel H, Sensoy O, Aksu EN, Gup R (2023) Synthesis,
703 structural investigations, DNA/BSA interactions, molecular docking studies, and anticancer
704 activity of a new 1,4-disubstituted 1,2,3-triazole derivative. ACS Omega 8:31839–31856.

705 Iacopetta D, Ceramella J, Catalano A, Saturnino C, Bonomo MG, Franchini C, Sinicropi
706 MS (2021) Schiff bases: interesting scaffolds with promising antitumoral properties. Appl
707 Sci 11:1877.

708 Jovanović S, Obrenčević K, Bugarčić ŽD, Popović I, Žakula J (2016) New bimetallic
709 palladium(II) and platinum(II) complexes: studies of the nucleophilic substitution reactions,
710 interactions with CT-DNA, bovine serum albumin and cytotoxic activity. Dalton Trans
711 45:12444–12457.

712 Kant R, Beri A, Mittal T, Bhalla Y, Saini R, Maji S (2024) Metal complexes with piperazine
713 ring based N2O2 ligands and their biological activity. Biointerface Res Appl Chem 14:139.

Kant R, Kaur T, Hilal Z, Aggarwal N, Maji S (2020) Synthesis and characterization of a series of phenyl piperazine based ligands. J Phys Conf Ser 153:012106.

Kant R, Maji S (2021) Recent advances in the synthesis of piperazine based ligands and metal complexes and their applications. Dalton Trans 50:785–800.

Kant R, Maji S (2023) Synthesis, characterization and biological evaluation of piperazine embedded copper complexes. Inorg Chim Acta 552:121515.

Kant R, Maji S (2024) Metal complex with piperazine ring-based ligand and their biological activities. Mater Today Proc. https://doi.org/10.1016/j.matpr.2024.04.034

Kant R, Saini R, Kaur M, Karnwal A, Rather HA, Maji S (2022) Synthesis and characterization of copper complexes of phenylpiperazine ring-based ligands and evaluation of their antimicrobial, BSA binding, computational, and molecular docking studies. J Phys Conf Ser 2267:012154.

Karthikeyan S, Chinnathambi S, Kannan A, Rajakumar P, Velmurugan D, Bharanidharan G, Aruna P, Ganesan S (2015) Investigation of optical spectroscopic and computational binding mode of bovine serum albumin with 1,4-bis((4-((4-heptylpiperazin-1-yl)methyl)-1H-1,2,3-triazol-1-yl)methyl)benzene. J Biochem Mol Toxicol 29:373–381.

Keypour H, Mahmoudabadi M, Shooshtari A, Hosseinzadeh L, Mohsenzadeh F, Gable RW (2017) Synthesis of Mn(II) and Zn(II) complexes with new macrocyclic Schiff-base ligands containing piperazine moiety: spectroscopic, structural, cytotoxic and antibacterial properties. Polyhedron 127:345–354.

Keypour H, Rezaeivala M, Valencia L, Pérez-Lourido P (2008) Synthesis and crystal structure of Mn(II) complexes with novel macrocyclic Schiff-base ligands containing piperazine moiety. Polyhedron 27:3172–3176.

Keypour H, Tafazzoli A, Farida SHM, Abdollahi-Moghadam M, Gable RW (2023) Synthesis, investigation of biological activities and theoretical studies of a novel hexaaza Schiff base ligand and its Ni(II) complex: X-ray crystal structure of the Ni(II) complex. Inorg Chem Commun 155:110981.

Khadir N, Boghaei DM, Assoud A, Nascimento OR, Nicotina A, Ghivelder L (2015) The structure, magnetism and EPR spectra of a (μ-thiophenolato)(μ-pyrazolato-N,N') double bridged dicopper(II) complex. Dalton Trans 44:2431–2438.

744 Kratz F (2008) Albumin as a drug carrier: design of prodrugs, drug conjugates and
745 nanoparticles. J Control Release 132:171–183.

746 Kumar S, Kumar N, Roy P, Sondhi SM (2014) Efficient synthesis of heterocyclic
747 compounds derived from 2,6-dioxopiperazine derivatives and their evaluation for anti-
748 inflammatory and anticancer activities. Med Chem Res 23:3953–3969.

749 Li G, Zhu D, Wang X, Su Z, Bryce MR (2020) Dinuclear metal complexes: multifunctional
750 properties and applications. Chem Soc Rev 49:765–838.

751 Malav R, Ray S (2025) Recent advances in the synthesis and versatile applications of
752 transition metal complexes featuring Schiff base ligands. RSC Adv 15:22889–22914.

753 Mondal K, Dey A, Mistri S (2023) Aminoethylpiperazine based metal Schiff base
754 complexes: catalytic and biological activities. Comments Inorg Chem 43:357–381.

755 Nafisi S, Bagheri Sadeghi G (2011) Interaction of aspirin and vitamin C with bovine serum
756 albumin. J Photochem Photobiol B 105:198–202.

757 Nekrasov DD (2001) Biological activity of 5- and 6-membered azaheterocycles and their
758 synthesis from α-aryl-2,3-dihydrofuran-2,3-diones. Chem Heterocycl Compd 37:291–304.

759 Nishat N, Haq MM, Ahamad T, Kumar V (2007) Synthesis, spectral and antimicrobial
760 studies of a novel macrocyclic ligand containing a piperazine moiety and its binuclear metal
761 complexes. J Coord Chem 60:85–96.

762 Otieno T, Rettig SJ, Thompson RC, Trotter J (1995) Pyridazine complexes of copper(II)
763 nitrate: synthesis and structural and magnetic studies. Inorg Chem 34:1718–1725.

764 Pait M, Kundu B, Kundu SC, Ray D (2014) Copper(II) complexes of piperazine based
765 ligand: synthesis, crystal structure, protein binding and evaluation of anti-cancerous
766 therapeutic potential. Inorg Chim Acta 418:30–41.

767 Priya MJ, Revanasiddappa HD, Setty PBS, Kumar HK, Chandan D, Shivamallu C, Abass
768 KS, Iqbal M, Amachawadi RG, Kollur SP (2025) New pyrazole-based Schiff base ligand
769 and its Ni(II) and Co(III) complexes as antibacterial and anticancer agents: synthesis,
770 characterization, and molecular docking studies. Main Group Met Chem 48:20250007.

771 Ragab MS, Soliman MH, Shehata MR, Shoukry MM, Ragheb MA (2022) Design,
772 synthesis, spectral characterization, photo-cleavage, and in vitro evaluation of anticancer

activities of new transition metal complexes of piperazine based Schiff base-oxime ligand. Appl Organomet Chem 36.

Ruede JE, Thornton DA (1976) The far infrared spectra of metal chloride complexes of pyridine in relation to their structures. J Mol Struct 34:75–81.

Rupesh KR, Deepalatha S, Krishnaveni M, Venkatesan R, Jayachandran S (2006) Synthesis, characterization and in vitro biological activity studies of Cu-M (M = Cu2+, Co2+, Ni2+, Mn2+, Zn2+) bimetallic complexes. Eur J Med Chem 41:1494–1503.

Sanjurani T, Paul S, Bharali DK, Barman P (2025) Investigation of disulfide-based Schiff base and its mono and binuclear Cu(II) complexes: green synthesis, crystal structure analysis, Hirshfeld surface analysis, in-vitro biological assessment, DNA binding studies, and computational studies. J Mol Struct 1335:141997.

Sharma PK, Makkar R (2017) Thiazine derivatives treated as potential antimicrobial agents. Asian J Pharm Clin Res 10:43–46.

Shebl M (2014) Synthesis, spectroscopic characterization and antimicrobial activity of binuclear metal complexes of a new asymmetrical Schiff base ligand: DNA binding affinity of copper(II) complexes. Spectrochim Acta A Mol Biomol Spectrosc 117:127–137.

Smith BC (2017) The C–O bond part I: introduction and the infrared spectra of alcohols. Spectroscopy 32:14–20.

Sodanapalli R, Nair R (2011) Synthesis and characterization of a pharmaceutical co-crystal: (aceclofenac). J Pharm Sci Res 3:1288.

Tan C, Liu J, Li H, Zheng W, Shi S, Chen L, Ji L (2008) Differences in structure, physiological stability, electrochemistry, cytotoxicity, DNA and protein binding properties between two Ru(III) complexes. J Inorg Biochem 102:347–358.

Turkyilmaz M (2017) Binuclear and mononuclear Cu(II) and Ni(II) complexes of tetra- and hexadentate ligands: synthesis, antifungal activity, spectroscopic and thermal characterization. J Therm Anal Calorim 129:451–460.

Uzun S et al (2019) Experimental and density functional theory (MEP, FMO, NLO, Fukui functions) and antibacterial activity studies on 2-amino-4-(4-nitrophenyl)-5,6-dihydrobenzo[h]quinoline-3-carbonitrile. J Mol Struct 1178:450–457.

803

804

805

Supplementary Files

This is a list of supplementary files associated with this preprint. Click to download.

- supplimentarydatabiological.docx